OFDM-based Joint Radar and Communication

Dylan Boland

A thesis submitted to University College Dublin in partial fulfillment

of the requirements for the degree of

Masters in Electronic and Computer Engineering

College of Engineering and Architecture

School of Electrical and Electronic Engineering

Supervised by: **Dr Nam Tran**

Date: April 24, 2022

Acknowledgements

I am very grateful to my supervisor Dr Nam Tran, for his unwavering guidance and encouragement over the course of the project. The meetings each and every week helped me to remain consistent, and to resolve problems that I was having more quickly. I also feel that I have learned a good deal about the thesis subject matter over the past eight months, owing hugely to my supervisor's advice and instruction.

I am also very grateful to my family who have supported me during my five years here in UCD: the dinners and lunches, the lifts to and from college, and the encouragement to continue on - it means a great deal to me.

Lastly, my friend group: I thank each of you for all the help and encouragement, and for enriching my college experience over the past few years. Memories of the occasions in which we've shared will only grow more precious as time flows on. I wish you all the best for the coming years.

Abstract

Over the past two decades the area of joint communications and radar has been actively researched from various angles. One of the main challenges in this area is the design of a waveform that is compatible for both communications *and* radar functionality, and one that meets with the present-day performance standards for each type of system. The development of such a waveform would give promise to the idea of combining the two functionalities into a single system. This is an inviting prospect for numerous reasons: firstly, a system that performs both functions would likely require less hardware, as components such as modulators and antennas could be shared. This would help in reducing costs, and the volume occupied when compared to two separate and dedicated systems. Secondly, it would allow for the frequency spectrum to be used more efficiently.

In this project, the method of Discrete Fourier Transform Spread (DFT-S) is shown, through simulations performed in MATLAB, to be compatible with correlation- and spectral estimation-based radar algorithms that use the orthogonal frequency-division multiplexing (OFDM) waveform. The performance with present-day wireless communications standards such as IEEE 802.11a and 802.11p is partly demonstrated.

Basic simulations of a MIMO-based OFDM radar are run through MATLAB. It appears to show that the use of multiple transmit antennas can help to increase the peak-to-sidelobes ratio at the receiver, making for an easier decision-making process.

Lay Abstract

This project is concerned with the design of signals that can be used in both communications and radar systems. By developing signals that can function in both communications and radar systems, the possibility of *combining* the two systems into one arises. This would likely reduce the production cost, as some of the electronic components might be common to both communications and radar systems, meaning they could be shared. If the final system has less hardware components, then it would likely occupy less space. As well as that, the combined system would be able to use the frequency spectrum more efficiently. This project also considers some different *ways* in which the signals may be processed so as to improve the overall performance.

Contents

List of Figures

Chapter 1

Introduction

1.1 Historical Developments of Wireless Communications and Radar Systems

Wireless communication is at the heart of a great number of the services that our society uses in day-to-day life. Such services include television and radio broadcasting [1], mobile communications [2], Wi-Fi [3], and satellite communications, to name some of the major ones. As for mobile communications, the evolution of the corresponding networks over the past three decades has helped in turning the once basic hand-held telephone into a small and powerful computer. Nowadays, one can do a great deal with a mobile phone: they can stream music and high-definition (HD) video; download and run applications (apps) that were once confined to desktop computers; browse the internet; and roam from one region of the world to another, with fewer connectivity issues. This evolution can be tracked from first generation

(1G) networks all the way up to the fifth generation (5G) ones that are in widespread use today. Some key changes occurred over these three decades that helped us to achieve the ultra-high data rates and low latency that we are now used to. The first 1G network was launched by Nippon Telegraph and Telephone in 1979 [4], to the citizens of Tokyo, Japan. Five years later, in 1984, the 1G network covered the entire nation, making Japan the first country to have nationwide 1G service. In 1983 Ameritech introduced 1G to the United States, and Motorola introduced the *Motorola DynaTAC* cell phone, which was the first commercially available cell phone for the public [4]. Fig. 1.1 shows a photo of the cell phone model. In 1G mo-

Fig. 1.1. The Motorola DynaTAC cell phone, launched in 1983.

bile networks, analogue-based technology that was centred around frequency-division

multiple access (FDMA) was used. The analogue-based technologies offered little security, a poor voice-call quality, and low speeds. Moreover, different regions of the world implemented the technology using different standards. As some examples, the United States and some countries of Asia used AMPS (Advanced Mobile Phone System), Nordic and Scandinavian countries employed NMT (Nordisk MobilTelefoni), the United Kingdom used TACS (Total Access Communications System), and Japan had JTACS (Japanese Total Access Communications System). One of the first key changes was seen in 2G, which opted for digital-based implementations over analogue-based ones. This afforded two big advantages: improved call security via encryption, and the introduction of text and multimedia messages through Short Message Service (SMS) and Multimedia Messaging Service (MMS); 2G also provided other advantages such as a better call quality, and an increase in download speed. Smaller mobile phones were also seen during the 2G era, spanning from around the 1990s, with Nokia bringing out mobiles such as the well-remembered Nokia 3210. The 2G service used standards such as the Global System for Mobiles (GSM), a digital version of AMPS called D-AMPS, and IS-95A. And these standards were based on time-division multiple access (TDMA) and narrowband code-division multiple access (CDMA), as well as FDMA. With the arrival of 3G in 2001 came new standards such as UMTS (Universal Mobile Telecommunications System) and CDMA2000, as well as wideband CDMA technology. The service also offered data speeds that were around four times faster than those of 2G, approaching 2 Mbits/s on average. The ability to browse the internet and stream music at a higher speed became available too. The 4G service offered yet more improvements, and many of the services

that we are accustomed to today such as high-quality video call and streaming, very fast internet access, online gaming, and high-definition videos. This era of mobile communications was also where smartphones became widespread, with the iPhone6 and Samsung Galaxy S4 being two of the most popular models. The 4G service also differed from previous generations in that it used orthogonal frequency-division multiplexing (OFDM) in tandem with multiple-input multiple-output (MIMO) technology in order to transfer data. This helped facilitate much higher data rates when compared to 3G. Lastly, and most recently, we have seen the introduction of the 5G service. Its implementation has brought about even higher data rates, much lower network latency, and an increased capacity for a larger number of connected devices - something which is especially promising for the Internet-of-Things (IoT) sector [5].

Another technology that has been crucial throughout recent history, and one that is becoming more present in the average person's day-to-day life, is radar. The basic concept of radar could be traced back to the classical experiments of Heinrich Hertz, the famous German physicist. Hertz, in the late 19th century, showed that radio waves can be reflected off metal objects - a possibility that was suggested by Maxwell's work on electromagnetism. However, it was not until the early 1930s that serious research and development of radar began. The major nations of the world - the United States, Great Britain, Germany, France, Italy, the Soviet Union, and Japan - began researching and developing ways to identify the approach of hostile aircraft. Fearing the possibility of war, Great Britain began research and development in 1935. By September of 1938, they had developed the first early-warning radar system: the *Chain Home*, a photo of which is shown in Fig. 1.2. It

Fig. 1.2. The Chain Home Radar Network in West Sussex, UK.

operated 24 hours a day, for the duration of the war, and helped the British to deploy their limited air force during the German air raids near the start of World War II (WWII). As for the United States, high-up members of the Navy were not hugely enthusiastic about radar until, in 1939, a monostatic radar was showcased at sea on the battleship *USS New York*. The monostatic setup meant that the same antenna could be used for transmission and reception. With the usefulness and feasibility of radar made clear, the U.S. Army began the development of radar in time for the commencement of WWII. Two of their initial systems were the (Signal Corps Radio no. 268) SCR-268 and the SCR-270, with the SCR-270 system being responsible for detecting the approach of Japanese bombers during the attack of 1941 on Pearl Harbor, Hawaii.

Although a great deal of the development of radar technology occurred during wartime, its continued evolution and application in many areas of day-to-day life is to be seen. The radar systems in modern-day cars allow them to gauge the distance and velocity of objects in their vicinity. This is being used to help reduce accidents, and to aid in the job of on-board units such as Adaptive Cruise Control (ACC) and

Blind Spot Detection (BSD). Radar systems are key to the industrial automation sector, where they help time-intensive and meticulous operations to be performed speedily and reliably. And weatherproof radar sensor technology also makes possible the use of self-driving farm machinery. This can help improve efficiency when it comes to large sectors of agricultural land, and it also mitigates the risk of accidents due to human fatigue.

1.2 Project Motivation

This project investigates further the possibility of designing waveforms that can jointly serve in communications and radar systems. For wireless communications, orthogonal frequency-division multiplexing (OFDM) is a method of data transmission that is very often employed. This is because OFDM has many advantages, such as an efficient implementation using the Inverse and Non-inverse Fast Fourier Transform (IFFT and FFT) algorithms, a high spectral efficiency, and its robustness to interference and frequency-selective channels. Due to the widespread use of the OFDM waveform in 4G and 5G communication systems, its potential use in radar applications has received a lot of attention and been an active area of research for many years. As such, OFDM-based waveforms will be focused on in this paper. A waveform that can be used to perform communications and radar functionality at the same time would give more strength to the idea of combining the two functions into a single system. This prospect is attractive for a few reasons. Firstly, the combined system would likely require less hardware, since both functions - radar

and communications - could share certain hardware components, such as transmit and receive antennas, modulators, radio-frequency (RF) oscillators etc. The reduced amount of hardware would also help to reduce production cost, something which is especially important when it comes to mass production. Secondly, by combining the two systems into one, there is the opportunity to more efficiently use the frequency spectrum. This potential benefit is promising given the increasing investment in the Internet-of-Things (IoT) sector, where more and more devices are wireless-based and integrated into single systems [6]. And this question about the feasibility of combining the two functions into a single system is a somewhat natural one as many of the systems that use radar technology also require communications capabilities, like with the automobile industry or industrial automation sector. Moreover, both radar and wireless communication systems are based on the principle of transmitting and receiving electromagnetic (EM) waves.

Chapter 2

Literature Review

The use of the OFDM waveform for radar purposes was considered as far back as 2000 in [7], but the communication function was of lesser focus and not considered in a general manner. The focus in [8], one of the first works concerning OFDM-based joint radar and communication (JCAR), focused solely on the *effect* of a radar setup on an OFDM-based communication system's bit error rate (BER) and throughput - radar sensing was not illustrated. Works such as [9] and [10] explore ways of improving the cross-correlation properties of the OFDM waveform for its use in radar processing. Although these works mention the application of OFDM in communications, the design of the waveform and signal-processing algorithms does not take into account much of the requirements of the communication functionality.

A fuller illustration of JCAR came with [11] in 2009. The authors advocate the use of a novel and direct symbol-based algorithm over correlation-based methods discussed in previous works. The algorithm performs an element-wise division between

the sequence of transmit and receive data symbols. This yields a sequence of samples of the channel's frequency response. Then, an Inverse Discrete Fourier Transform (IDFT) operation is performed on the result, and the sampled channel impulse response is obtained - the peak in the channel's discrete-time impulse response provides an estimation of the propagation delay. The authors point out that this algorithm is *independent* of the data transmitted, as it eliminates the transmitted data *before* carrying out further processing. This is not the case with correlation-based approaches, where, due to random correlations in the transmitted data, unwanted or misleading sidelobes can appear in the range-Doppler map [12], [13], meaning the performance is dependent on the transmitted data symbols. The feasibility and effectiveness of this symbol-based algorithm is tested and verified in [13] from 2010, using real-world experiments. The symbol-based approach is elaborated on further by two of the same authors from [11] in [12]. The transmit and receive sequences are converted to a matrix form and considered as *frames* made up of symbols, with each column of a frame representing an OFDM symbol. Like in [11], the element-wise division between the two is taken, thereby removing the dependency on the transmitted data. A two-dimensional Fourier transform is then computed on the resulting matrix in order to yield the range-Doppler map, where estimation of the delay and Doppler shift can be made.

In [14], the author discusses, among other methods, a two-dimensional periodogram-based algorithm. Like the symbol-based approach in [11], [13], the algorithm computes the element-wise division between the transmit and receive frames, before further processing which ultimately yields a range-Doppler map, where peaks in

the map correspond to potential targets. The author suggests that this algorithm makes more efficient use of the structure of the OFDM signal when compared to correlation-based approaches. It is also pointed out that the algorithm can be implemented efficiently on hardware platforms such as Field Programmable Gate Arrays (FPGAs), owing to its small memory footprint, and the efficiency of the FFT and IFFT algorithms.

Different correlation-based OFDM radar receivers are discussed in [15]. The algorithms are based on the two-dimensional cross-correlation between the received signal and shifted replicas of the transmitted one. The first receiver analysed is based on matched filtering (MF), and the corresponding expression has a high computational complexity. As a result, the authors, inspired by [9], propose the use of a *proximate* matched filter (PMF) in order reduce the computational complexity and allow for efficient implementation using the FFT and IFFT algorithms. The performance of this PMF receiver is then investigated *after* the cyclic prefix (CP) is first removed - the authors use the acronym PMF-CP for this receiver.

The authors in [15] also discuss approaches based on *reciprocal* filtering (RF), which process the received sequence and the reciprocal of the transmitted sequence. As is discussed and shown in [15], when a unit-amplitude modulation scheme is used the approaches based on RF become equivalent to the MF methods initially presented in the work. Like with the MF approaches, an investigation of the performance of RF approaches after the CP is removed from each received OFDM symbol is also investigated. Like with the proximate matched filter, a proximate reciprocal filter is suggested as it allows for more efficient and practical implementation.

Chapter 3

Background

3.1 Orthogonal Frequency-Division Multiplexing

Orthogonal frequency-division multiplexing (OFDM) is a method of data transmission that is widely employed nowadays: it is used in mobile communications, and has been adopted for fourth generation (4G), and fifth generation (5G) systems [16]; it is used in wireless local-area networks (WLANs) [17], [18]; digital video broadcasting (DVB) [1] and digital audio broadcasting (DAB) [19]; and even visible-light communications (VLC) [20], [21]. The success of the OFDM scheme and its widespread use is down to its many inherent advantages: it has a high spectral efficiency, it is more resistant to frequency-selective channels than single-carrier schemes, it is robust against inter-symbol interference (ISI), and it can still facilitate very high data rates. These are just some of its main advantages.

An OFDM symbol is comprised of a given number (N) of partly overlapping and

mutually orthogonal subcarriers. The orthogonality ensures that the neighbouring subcarriers do not interfere with one another, while still allowing for the data associated with each subcarrier to be retrieved at the receiver (Rx). The orthogonality condition is met by using a subcarrier spacing, denoted by Δf, that is equal to the inverse of the symbol duration T. Moreover, since the subcarriers are partly overlapping, less of the frequency spectrum is occupied when compared to a standard frequency-division multiplexing (FDM) scheme, which uses a frequency *guard* band to mitigate the problem of inter-channel interference (ICI). This is illustrated in Fig. 3.1, and is the reason why the OFDM scheme is considered to use the spectrum efficiently. A set of N symbols $\{c_0, c_1, ..., c_{N-1}\}$ - obtained from a modulation

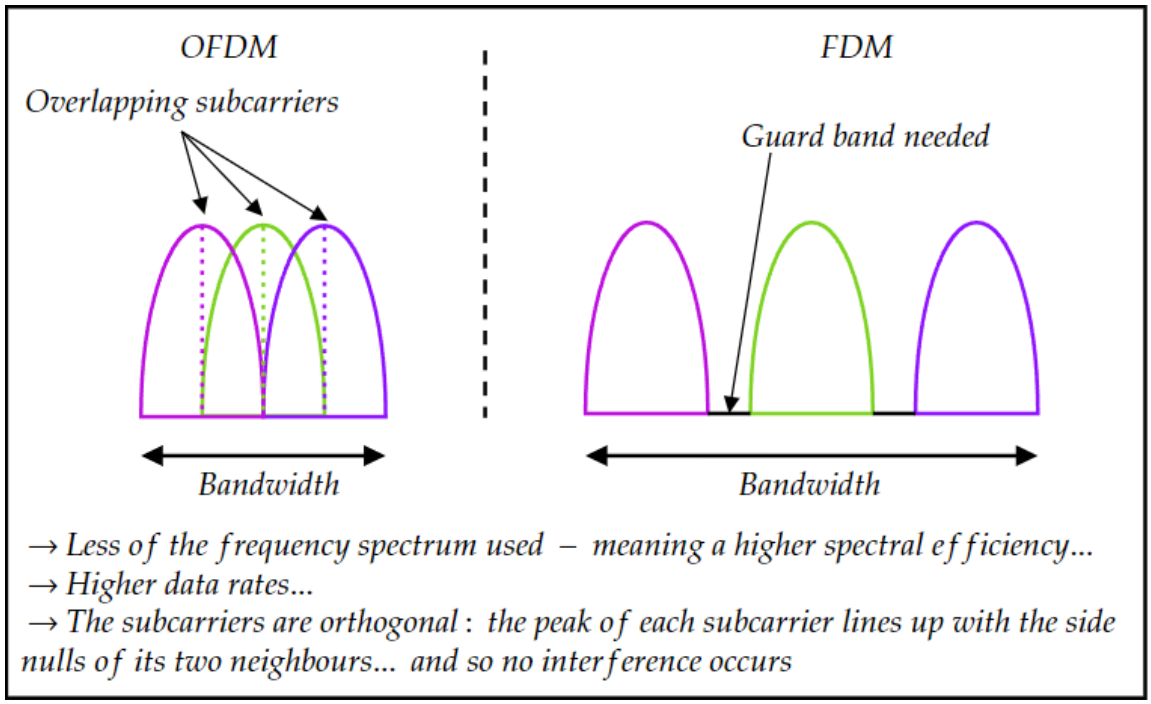

Fig. 3.1. A comparison of the use of bandwidth in OFDM and FDM.

alphabet such as BPSK, QPSK, 16-QAM, or 64-QAM - is then used to modulate each of the N subcarriers, with c_0 modulating the first subcarrier, also known as the *DC* subcarrier, c_1 modulating the second subcarrier, and so on. An OFDM symbol (s) in continuous time may be described by

$$s(t) = \sum_{k=0}^{N-1} c_n e^{j2\pi k\Delta f t}, \tag{3.1}$$

with $k\Delta f$ being equal to the frequency offset of the k-th subcarrier. By sampling $s(t)$ with a period of $T_s = T/N$, and introducing the discrete-time index variable n, so that $t = nT_s$, a discrete-time representation of an OFDM symbol can be obtained as

$$s(nT_s) \triangleq s(n) = \sum_{k=0}^{N-1} c_k e^{j2\pi k\Delta f(n\frac{T}{N})} = \sum_{k=0}^{N-1} c_n e^{j2\pi k\frac{n}{N}}. \tag{3.2}$$

Equation (3.2) represents the Inverse Discrete Fourier Transform (IDFT) of the set of modulation symbols $\{c_0, c_1, ..., c_{N-1}\}$. Moreover, the IDFT operation can be computed very efficiently using the Inverse Fast Fourier Transform (IFFT) algorithm, meaning that the OFDM modulation process is all-digital and efficient to implement in hardware. The symbols that are modulated onto the subcarriers are normally of three main types: information-bearing symbols, null symbols, or *pilot* symbols. The DC subcarrier is typically not used during transmission, and is therefore modulated with a null symbol (zero value). Particular subcarriers can be assigned to pilot *tones* or symbols, and then the receiver side, aware of *which* subcarriers are carrying the pilot tones, can perform channel estimation based on *how* the channel has affected

the transmitted pilot symbols. There are different methods of pilot-tone insertion, with two common approaches being block-type and comb-type [22]. In the comb-type approach, pilot symbols are evenly spaced among the subcarriers. Fig. 3.2 attempts to illustrate the insertion of two pilot tones on the transmitter side. The remaining subcarriers, excluding the DC subcarrier, are loaded with data-bearing symbols.

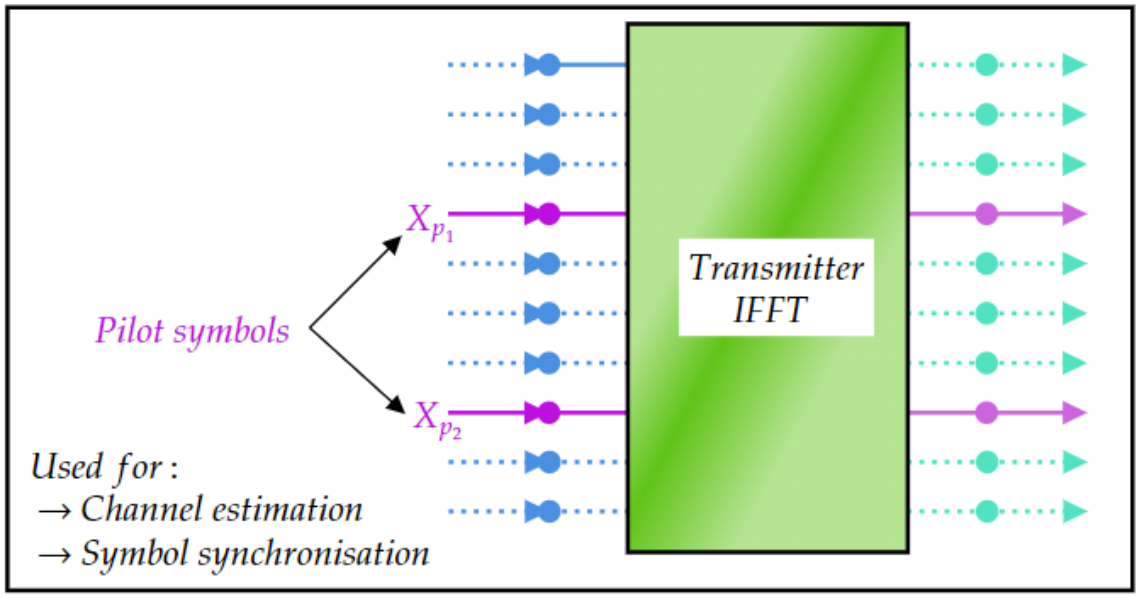

Fig. 3.2. Pilot tones or symbols being loaded onto two subcarriers.

The Cyclic Prefix (CP)

One of the key attributes of the OFDM scheme is the *cyclic prefix* (CP), which acts as a guard interval (GI), and helps to combat the problem of inter-symbol interference (ISI) at the receiver. ISI occurs when transmitted symbols interfere with one another at the receiver. This is often caused by the multipath delay of the channel, which

leads to copies of a transmitted symbol arriving at the receiver out of sync. Symbols sent at one point in time can be corrupted, at the receiver, by copies of symbols that were sent before or later in time. This can corrupt the payload, leading to a significant bit error rate (BER) in the communication system. In order to give more motivation as to why the cyclic prefix is needed, Fig. 3.3-3.4 depicts what could happen if it were not included. The process of adding the CP consists in prefixing

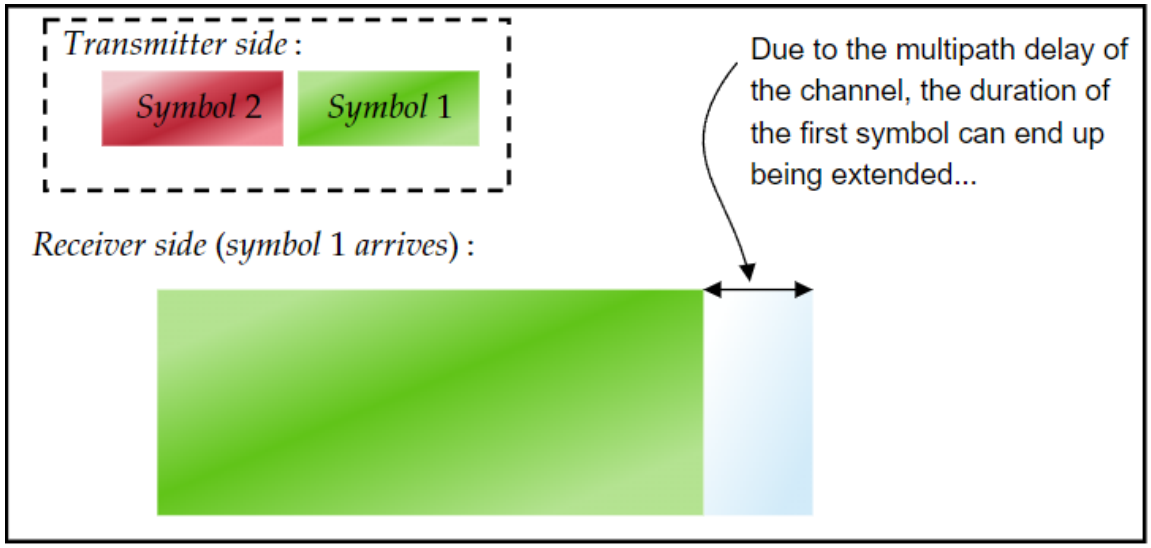

Fig. 3.3. OFDM symbol 1 arrives at the Rx.

an end section of a symbol to its front. This has the consequence of making each symbol appear cyclical to the receiver. Let the fraction of the OFDM symbol that is copied and prefixed be G. Therefore, the extended symbol length, *after* the CP has been added, is $N + GN$. The guard interval duration (T_G) is equal to GT, meaning the extended OFDM symbol duration is $T_O = T + GT$. Fig. 3.5-3.6 attempts to illustrate more clearly how the CP actually protects the payload data. The basic

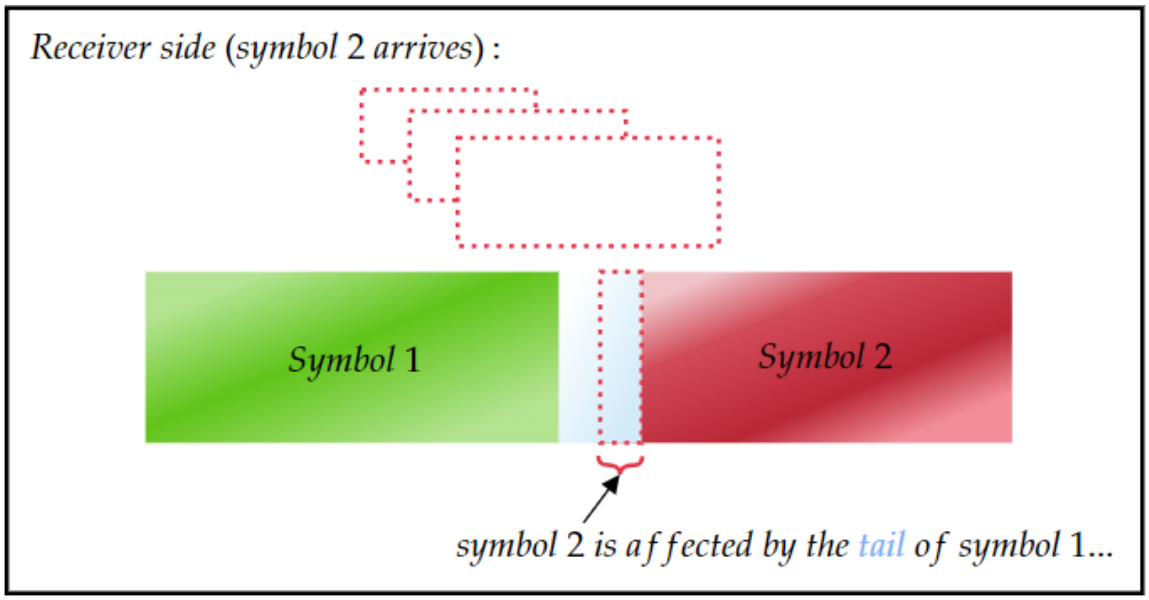

Fig. 3.4. OFDM symbol 2 arrives at Rx and is affected by the tail of symbol 1.

idea is that if the CP length is as long as the maximum delay associated with the channel, then any interference that occurs will be between the tail of one symbol and the CP of the next symbol. As the CP is a copy of the end of a given symbol, it is not a severe problem if it is corrupted on reception, as the receiver tends to discard this part of each symbol anyway. In this way, the payload data is protected. Typically, the CP is chosen to be a little bit longer than the expected maximum delay of the communication channel - making it too much longer would reduce the communication data rate. Fig. 3.7 attempts to illustrate why the CP needs to be *at least* as long as the maximum path delay of the channel. If it is insufficient in length, then the payload data of the symbol is still affected, leading to bit errors.

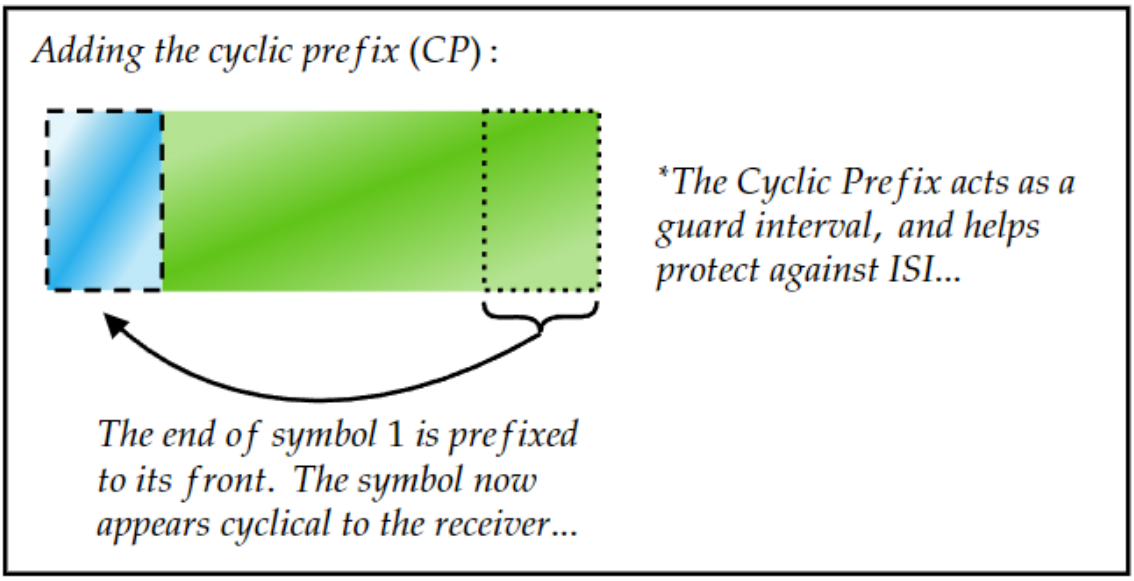

Fig. 3.5. Adding the cyclic prefix (CP).

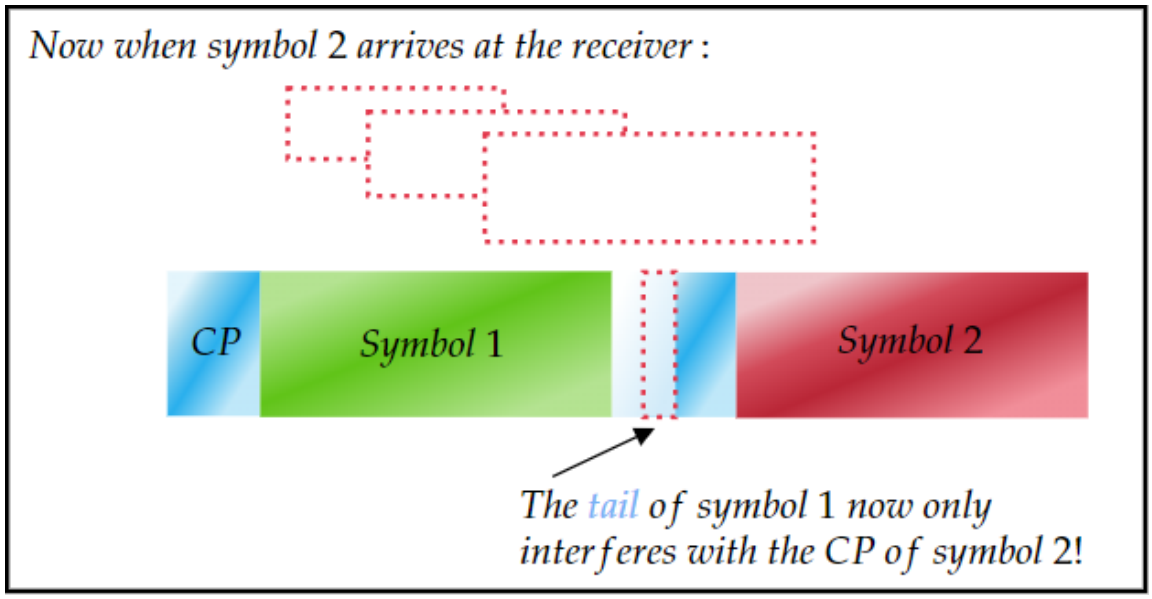

Fig. 3.6. The CP guards the payload data of symbol 2.

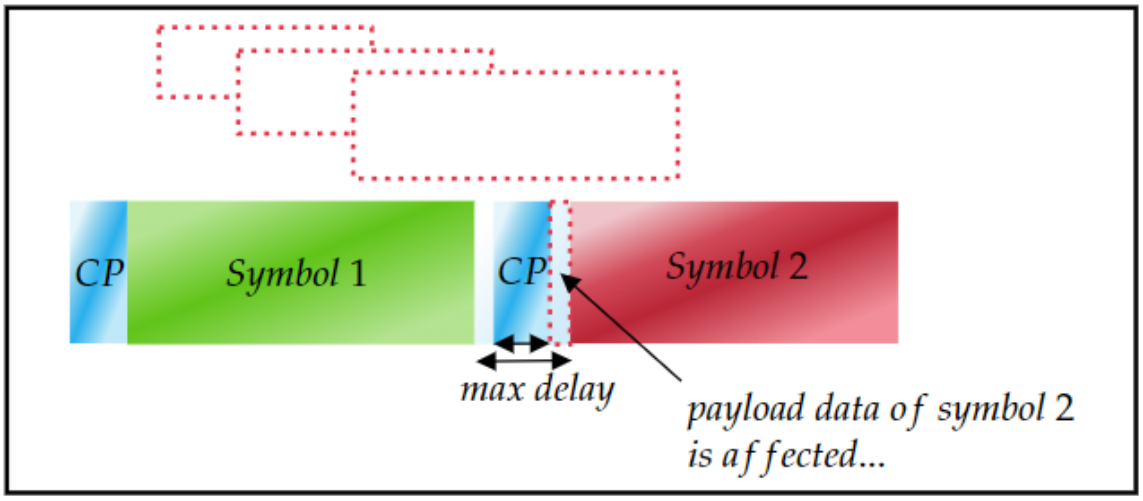

Fig. 3.7. CP is not sufficiently long.

Frequency-domain Equalisation

Another benefit of the OFDM scheme is that it is relatively easy to perform *frequency-domain equalisation* (FEQ) at the receiver, a process which helps to combat the negative effect of the channel on the transmitted symbols. Due to the addition of the CP, the output of the channel becomes the *circular* or *cyclical* convolution between the input (x_n) and the channel's impulse response (h_n), overlaid with white Gaussian noise (w_n), as in (3.3).

$$y_n = x_n \circledast h_n + w_n. \tag{3.3}$$

The Fourier transform is linear, and the *convolution theorem* dictates that a convolution in the time domain is equivalent to multiplication in the frequency one. This

allows (3.3) to be equivalently re-expressed in the frequency domain as

$$Y_k = X_k H_k + W_k. \tag{3.4}$$

From (3.4) the channel gain at the k-th subcarrier can be expressed as

$$H_k = \frac{Y_k}{X_k} - \frac{W_k}{X_k}. \tag{3.5}$$

The receiver will not know what symbols were loaded onto most of the subcarriers, but it will for the subcarriers assigned to pilot tones. Therefore, the channel gains can be estimated for *these* subcarriers. Let X_{P_1} be the first pilot symbol inserted at the transmitter, and Y_{P_1} be the corresponding received pilot symbol. The channel gain at the subcarrier frequency associated with this pilot tone can be estimated as

$$\hat{H}_{P_1} = \frac{Y_{P_1}}{X_{P_1}}. \tag{3.6}$$

Demodulation at the receiver is performed very efficiently using a Fast Fourier Transform (FFT) block, yielding the received pilot and data symbols - an illustration of this is shown in Fig. 3.8. Interpolation can then be used to estimate the channel gains at the other subcarrier frequencies - an attempt to illustrate this, using arbitrary numbers and labels, is shown in Fig. 3.9. The received data symbols can then be loaded into a block that performs the equalisation process - this is illustrated, to some degree, in Fig. 3.10.

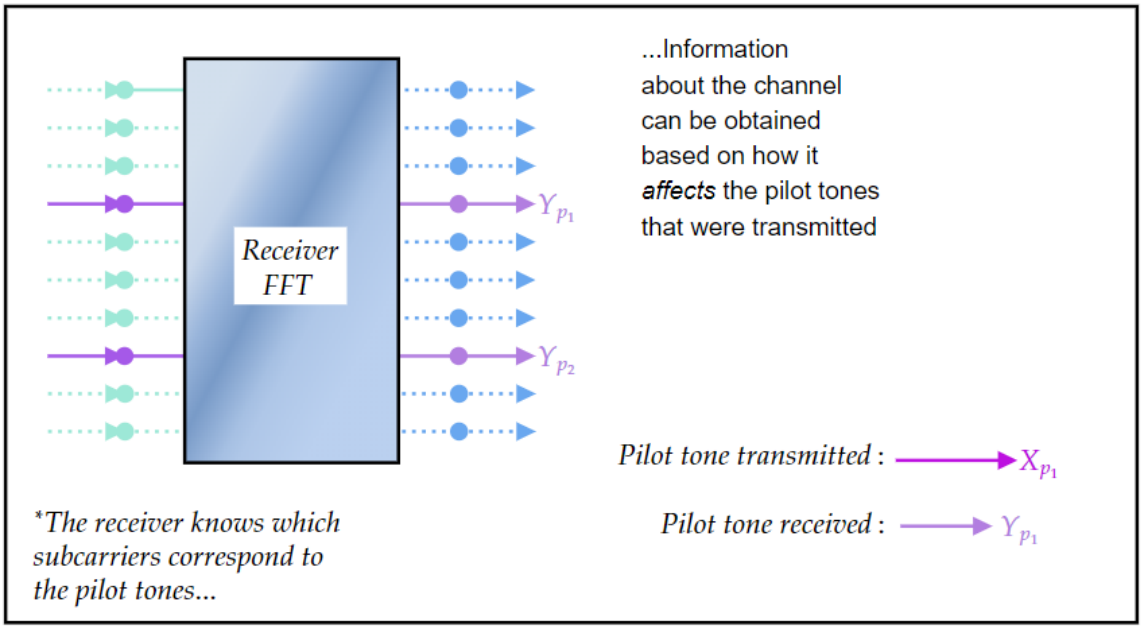

Fig. 3.8. OFDM demodulation using an FFT block.

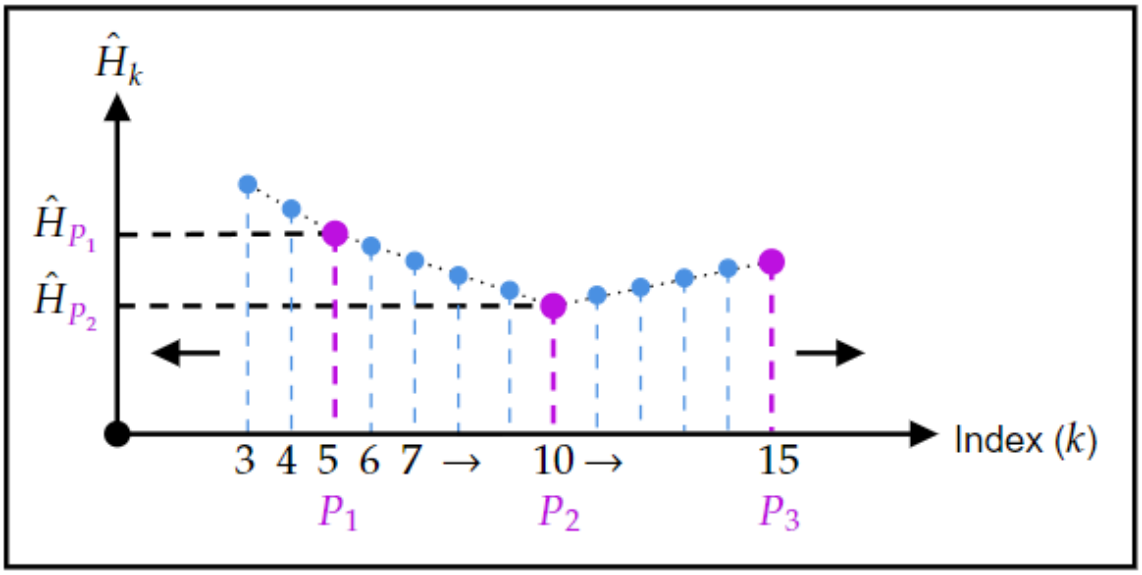

Fig. 3.9. Interpolation of channel gains at data subcarrier indexes.

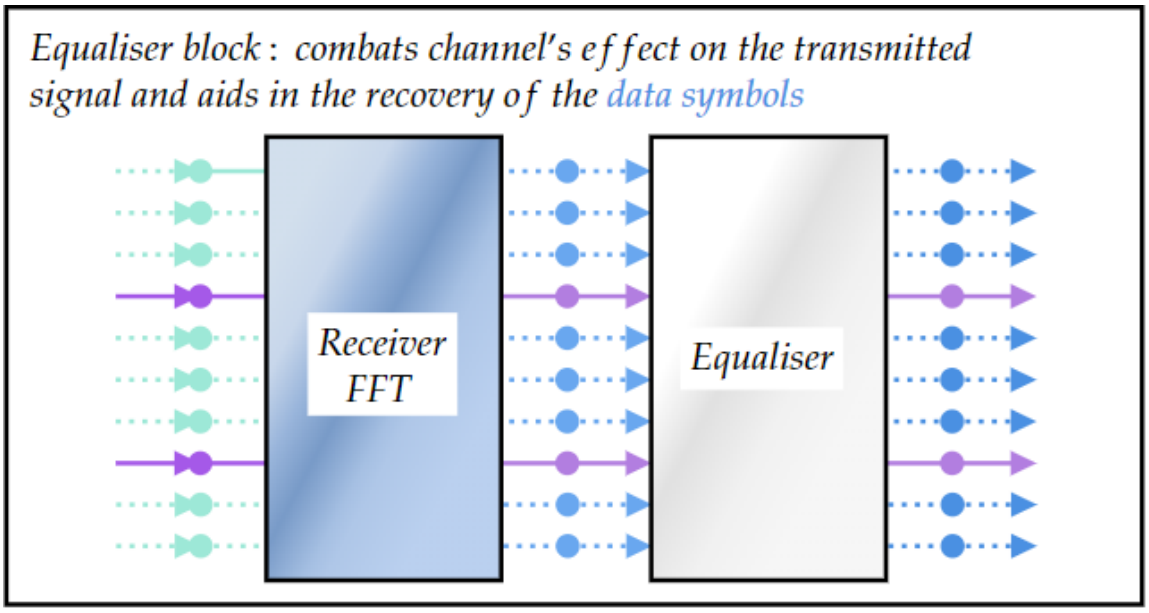

Fig. 3.10. Equalisation block in the receiver chain.

If the symbol Y_k is received on the k-th subcarrier, and if the channel gain is estimated as being $\hat{H}_k$, then an estimation of the transmitted symbol ($\hat{X}_k$) may be made in accordance with (3.7).

$$\hat{X}_k = \frac{Y_k}{\hat{H}_k}. \tag{3.7}$$

Peak-to-Average Power Ratio

One of the main drawbacks of the OFDM waveform is its high peak-to-average power ratio (PAPR), which is induced by the Inverse Fast Fourier Transform (IFFT) block used in the transmitter (Tx). This high PAPR requires the high-power amplifier (HPA) used by the transmitter to have a highly linear characteristic, so as to avoid

distortions of the waveform during transmission [23]. Distortion of the waveform during transmission is very undesirable as it can lead to an increase in the communication system's bit error rate [24]. As well as distortions, the high PAPR of the waveform can lead to a high power consumption in the user equipment (UE) used during uplink transmissions. A high power consumption can pose a challenge to the battery life of small and mobile devices. The PAPR of an OFDM symbol (s) may be expressed by

$$PAPR = \frac{\max\limits_{mT \geq t \leq (m+1)T} [|s(t)|^2]}{\mathbb{E}\left[|s(t)|^2\right]}. \tag{3.8}$$

Various methods to combat the high PAPR of the OFDM waveform have been analysed in the literature. Some examples of the more common methods are selective mapping (SLM) [25], [26], tone reservation (TR) [27], tone injection (TI), and the Discrete Fourier Transform Spread (DFT-S) technique [28], [29]. The last method mentioned, DFT-Spread (DFT-S), is a point of focus in this paper.

3.2 MIMO

In this section, a brief overview of Multiple-Input Multiple-Output (MIMO) technology will be given. MIMO technology is widely used nowadays, such in Wi-Fi communications, as well as 3G, 4G, 4G LTE, and 5G communications systems. It provides the ability for multiple data signals to be transmitted over a communication link simultaneously, thereby allowing for very high data rates to be achieved. The Shannon-Hartley theorem dictates that if the channel bandwidth is fixed and the

signal-to-noise ratio (SNR) cannot be increased, then the maximum channel capacity is more or less fixed too. In an open environment, signals transmitted from an array of antennas typically have many paths to the receiver, each with different delay times. This can lead to copies of signals arriving at the receiver and causing interference. MIMO technology capitalises on the multipath environment by considering the various paths from the transmitter to receiver as an extra *spatial* dimension. This can allow for the channel capacity to potentially be increased further, without also requiring an increase in the channel bandwidth. Fig. 3.11-3.12 is a basic illustration of a three-antenna array, and the many reflected signals that might occur off typical objects in an urban environment. Since the various paths through the

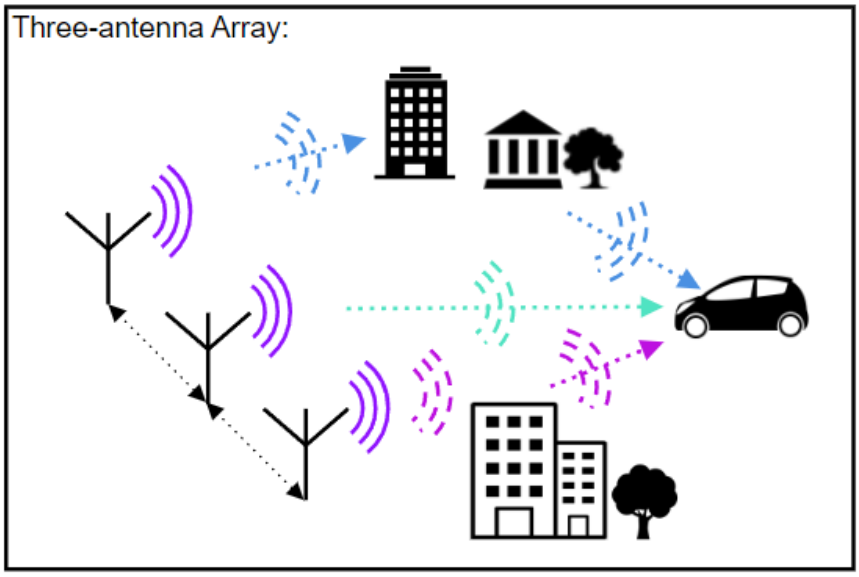

Fig. 3.11. Three antennas transmitting the same signal into an urban environment.

environment have different delays, the transmitted signals can arrive at the receiver out of sync, and at different times. This effect can be used to estimate the position

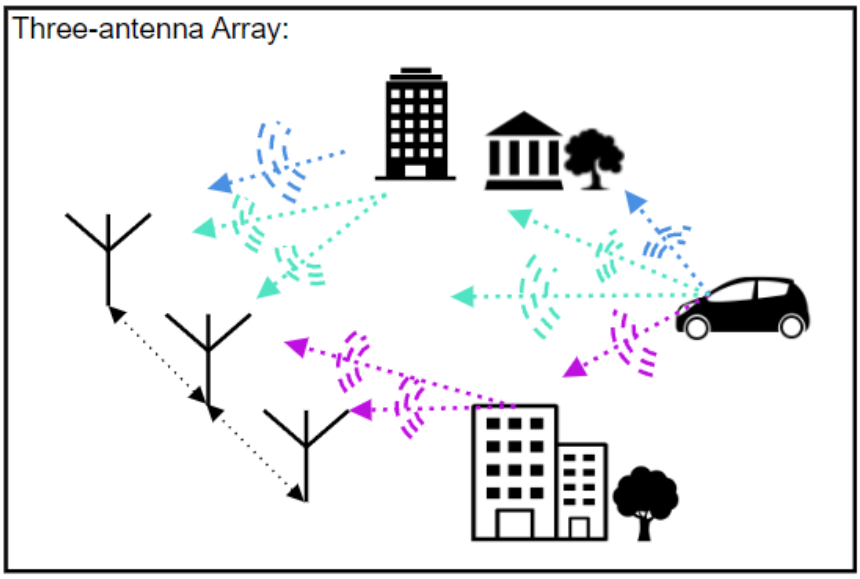

Fig. 3.12. Antennas can receive reflections of signals that they did not transmit.

of a transmitter, as well as the angle of arrival (AoA) [30] of an incoming signal.

MIMO radar has also be actively researched for many years [31], [32], [12]. One broad and simple approach to processing the many received signals is the following: cross-correlate each received signal with shifted replicas of the transmitted one, and then combine the results of each of these cross-correlations in some way, so as to hopefully yield improved results. In [12], approaches based on the Fourier transform and Multiple Signal Classification (MUSIC) are presented and analysed. The MUSIC algorithm is considered to be more complex, but yields a higher angular resolution.

Chapter 4

OFDM Radar Algorithms

There are many types of radar algorithms, but each shares a common goal: identify targets in the surroundings. More specifically, two pieces of information are normally desired: the distance to the target, and the velocity of the target. The basic principle of operation in a radar is that an electromagnetic (EM) wave is sent out by the transmitter (Tx), the signal impinges on any objects in the environment, and is then reflected back towards the transmitter. The distance to the target can be estimated based on the total propagation time, denoted by τ, and the velocity of the target can estimated by calculating the difference in frequency of the reflected signal when compared to the transmitted one. This is known as the *Doppler shift*, and is often denoted by f_D. The relationship between the Doppler shift and the velocity of the target is given by

$$f_D = \frac{2v_t f_C}{c}, \tag{4.1}$$

where v_t represents the velocity of the target, f_C is the central frequency of the transmitted EM wave, and c denotes the speed of light. Equation (4.1) is derived from the expression for the Doppler effect in the case of an EM wave, under the assumption that the target's velocity will be *negligible* when compared to the speed of light. If the radar system is imagined to be moving, then v_t is likely better replaced by v_{rel}, to denote the relative velocity between the radar transmitter and the target. The propagation time may be computed by

$$\tau = \frac{2d}{c}. \tag{4.2}$$

By estimating f_D and τ at the receiver, (4.1) and (4.2) can then be used to obtain information about the target's velocity and distance, as illustrated further in Fig. 4.1. The reflected signal off a moving target is a delayed-in-time and shifted-in-frequency

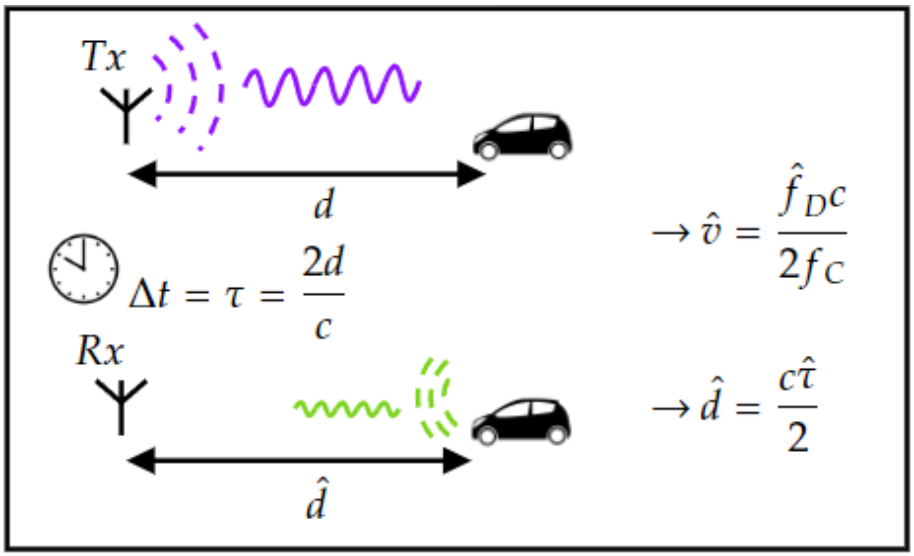

Fig. 4.1. An EM wave is transmitted and then reflected off a vehicle.

version of the transmitted one, and can be expressed as

$$r(t) = \alpha s(t - \tau) e^{j2\pi f_D t}, \tag{4.3}$$

where $r(t)$ represents the received signal, $s(t)$ is the transmitted signal, and α is the signal attenuation caused by the target. As is seen in (4.3), the signal (r) is delayed in time by an amount that is equal to the propagation delay, τ. The positive sign in the exponential term signifies that the received signal has a positive Doppler shift, and its frequency is greater than that of s - this corresponds to the target moving towards the transmitter, or vice versa; a negative Doppler shift occurs when the transmitter and target are moving apart.

4.1 Digital Signal Processing (DSP) Algorithms

The analog or continuous-time signal that arrives at the receiver front end is sampled by an analog-to-digital converter (ADC), resulting in a digital signal that can be further processed. One of the principal benefits of working with digital signals is that the samples may be processed in the time *or* frequency domain. In Fig. 4.2, which illustrates part of a basic transmitter and receiver chain for an OFDM-based system, there are three pairs of sequences labelled (1), (2), and (3). Many of the radar receivers discussed below process samples of the transmit and receive sequences in the frequency domain, i.e., they process the complex data symbols going into the transmit-side IDFT block and those retrieved from the receive-side DFT block. These sequences are pointed to by the double-ended arrow labelled (3) in Fig. 4.2. It is

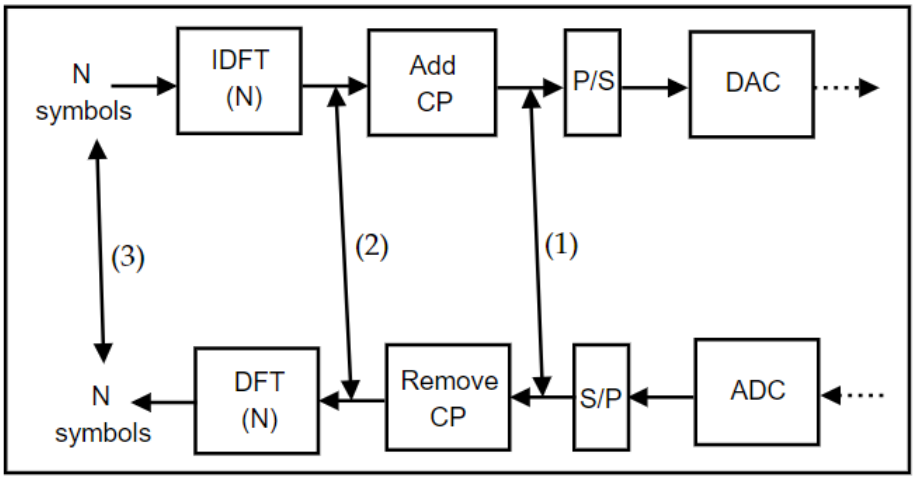

Fig. 4.2. Part of the transmitter and receiver block diagram. Labels (1) to (3) denote the points at which samples might be processed by a DSP algorithm.

not shown in Fig. 4.2, but some of the algorithms that process frequency-domain samples retain the cyclic prefix (CP).

In order to introduce the expressions for the subsequent receivers with more ease, a useful matrix notation which is discussed in detail in [33, 34] is first introduced. During transmission, OFDM symbols are sent in bursts, where a burst of symbols can be considered as a *frame*. The matrix notation conveniently captures the structure of a frame, in that each of the M columns of the matrix represents an OFDM symbol, and each of the N rows corresponds to one of the subcarriers. In this way, the element on row k and column m represents the data or pilot symbol transmitted or received on the k-th subcarrier in the m-th OFDM symbol, depending on whether it is the transmit or receive frame under inspection. The transmitted frame may be

expressed by

$$\mathbf{F_{Tx}} = \begin{pmatrix} c_{0,0} & c_{0,1} & \cdots & c_{0,M-1} \\ c_{1,0} & c_{1,1} & \cdots & c_{1,M-1} \\ \vdots & \vdots & \ddots & \vdots \\ c_{N,0} & c_{N,1} & \cdots & c_{N,M-1} \end{pmatrix} \tag{4.4}$$

and the received frame by

$$\mathbf{F_{Rx}} = \begin{pmatrix} b_{0,0} & b_{0,1} & \cdots & b_{0,M-1} \\ b_{1,0} & b_{1,1} & \cdots & b_{1,M-1} \\ \vdots & \vdots & \ddots & \vdots \\ b_{N,0} & b_{N,1} & \cdots & b_{N,M-1} \end{pmatrix}. \tag{4.5}$$

The data symbols in $\mathbf{F_{Rx}}$ can then be processed at the receiver in order to estimate the propagation delay and Doppler shift.

4.2 Periodogram-based Algorithm

The first algorithm presented here is a periodogram-based one that is discussed in far greater detail in [14]. First, the received frame is expressed in terms of the transmitted frame. This is achieved by considering how a given data symbol $c_{k,l}$ is affected by the propagation delay (τ) and Doppler shift (f_D), resulting in the corresponding received data symbol $b_{k,l}$. As the author in [14] points out, it can be useful to think of each row of $\mathbf{F_{Tx}}$ as a discrete-time signal, with a sampling period of

T_O, representing the extended OFDM symbol duration. This is the same as the time between the sending of two consecutive OFDM symbols. An attempt to illustrate this idea can be seen in Fig. 4.3.

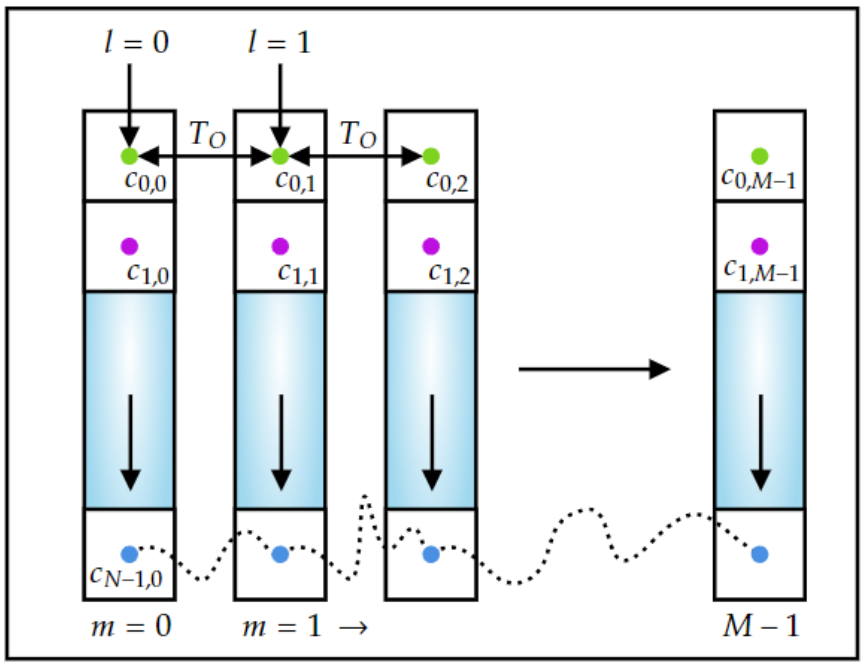

Fig. 4.3. Each row of the frame can be thought of as a signal sampled every T_O seconds.

This leads to the formulation given for the effect of the Doppler shift, which is that it may be viewed as the modulation of each row of $\mathbf{F_{Tx}}$ by a discretely-sampled complex sinusoid, given by

$$e^{j2\pi f_D l T_O},$$

where l is a discrete-time index variable. The complex sinusoid above can be obtained

by allowing $t = lT_O$ in $e^{j2\pi f_D t}$, which is the exponential term that appears in the expression for $r(t)$ in (4.3). Next, the formulation for the effect of the propagation delay is given, which is that it causes a phase shift to each of the transmitted symbols $c_{k,l}$, with the phase shift able to be expressed as

$$e^{-j2\pi f_k \tau} = e^{-j2\pi(f_0 + k\Delta f)\tau},$$

with f_k representing the frequency of the k-th subcarrier, equivalent to the frequency of the first subcarrier, f_0, plus the offset of $k\Delta f$. The two effects - that of the propagation delay and that of the Doppler shift - are then used to arrive at the expression for a symbol of the received frame in terms of the symbol in the transmitted frame as

$$(\mathbf{F_{Rx}})_{k,l} = \alpha(\mathbf{F_{Tx}})_{k,l} \cdot e^{j2\pi f_D l T_O} \cdot e^{-j2\pi(f_0 + k\Delta f)\tau} + (\mathbf{W})_{k,l}, \tag{4.6}$$

with $(\mathbf{W})_{k,l}$ representing a complex-valued white Gaussian noise matrix with a mean of zero, and α representing the signal attenuation, as in (4.3). At this point, the transmitted data is eliminated by performing an element-wise division of $(\mathbf{F_{Rx}})_{k,l}$. This is done by dividing both sides of (4.6) by the transmitted frame. The resulting matrix, denoted by $\mathbf{F}$ in [14], may be expressed as

$$(\mathbf{F})_{k,l} = \frac{(\mathbf{F_{Rx}})_{k,l}}{(\mathbf{F_{Tx}})_{k,l}} = \alpha e^{j2\pi f_D l T_O} \cdot e^{-j2\pi(f_0 + k\Delta f)\tau} + \frac{(\mathbf{W})_{k,l}}{(\mathbf{F_{Tx}})_{k,l}}. \tag{4.7}$$

The matrix $\mathbf{F}$ is then processed in the following way: an FFT of each row is computed,

followed by an IFFT operation on each column. As is mentioned, the size of the FFT taken can be greater than M, the number of columns in $\mathbf{F}$. This implies that zero padding is used. Likewise, the size of the IFFT operation along each column can be greater than N, the number of rows in $\mathbf{F}$. This zero padding along each dimension helps to improve the frequency resolution, although it does increase the size of the computations. Lastly, the square of the magnitude of each element of the resulting matrix is taken, yielding the two-dimensional periodogram. Peaks in the periodogram correspond to potential targets. The bin indexes can be converted to estimates of τ and f_D using

$$\tau_k = \frac{k}{N_{IFFT}\Delta f},\ k = 0,\ 1, ...,\ N_{IFFT} - 1 \tag{4.8}$$

$$f_{D_l} = \frac{l}{M_{FFT}T_O},\ l = -\frac{M_{FFT}}{2}, ...,\ \frac{M_{FFT}}{2} - 1. \tag{4.9}$$

The derivations of (4.8) and (4.9) are detailed in [33], [14]. In order to reduce the amount of computations that are needed to obtain the periodogram from $\mathbf{F}$, the author discusses that a *search* range *within* the periodogram can be defined [33], [14]. The number of rows in the periodogram (N_{IFFT}) can be cropped to $N_{max} = GN_{IFFT}$, where G is the fraction of an OFDM symbol that is used for the cyclic prefix (CP). In a similar way, the number of columns may be reduced from M_{IFFT} to $M_{max} = DM_{IFFT}$. Where D is a fraction, typically around 1/10 [33].

4.3 Correlation-based Algorithms

The other broad type of radar algorithms are based on the idea of cross-correlating the received signal, $r(t)$, with shifted replicas of the transmitted signal, $s(t)$, in order to obtain estimates for τ and f_D. This process may be expressed by

$$\chi_{r,s}(\tau, f) = \int_{-\infty}^{+\infty} r(t)s^*(t-\tau)e^{-j2\pi ft}dt. \tag{4.10}$$

By computing the cross-correlation value, $\chi_{r,s}$, at various values of (τ, f) an intensity map or *ambiguity* surface can be generated. Peaks in the intensity map correspond to signals which correlate highly with the received signal. From these peaks, estimates of the delay and Doppler shift associated with r can be made. As is mentioned in [35], a discrete version of (4.10) is obtained after sampling is performed at the receiver. The two-dimensional cross-correlation can also be computed in a block-by-block manner, by segmenting the received sequence r into "blocks", where each block is an OFDM symbol - an attempt to illustrate this is shown in Fig. 4.4. It is assumed that M OFDM symbols are transmitted in a burst, with each symbol comprising N subcarriers. The variable d denotes the delay in discrete time. The matrix notation for representing an OFDM frame (4.4 and 4.5) can be used again. Let s_m be the m-th transmitted OFDM symbol, and r_m be the m-th received OFDM symbol - i.e.,

$$s_m = [c_{0,m}, c_{1,m}, c_{2,m}, ..., c_{N-1,m}], \tag{4.11}$$

$$r_m = [b_{0,m}, b_{1,m}, b_{2,m}, ..., b_{N-1,m}]. \tag{4.12}$$

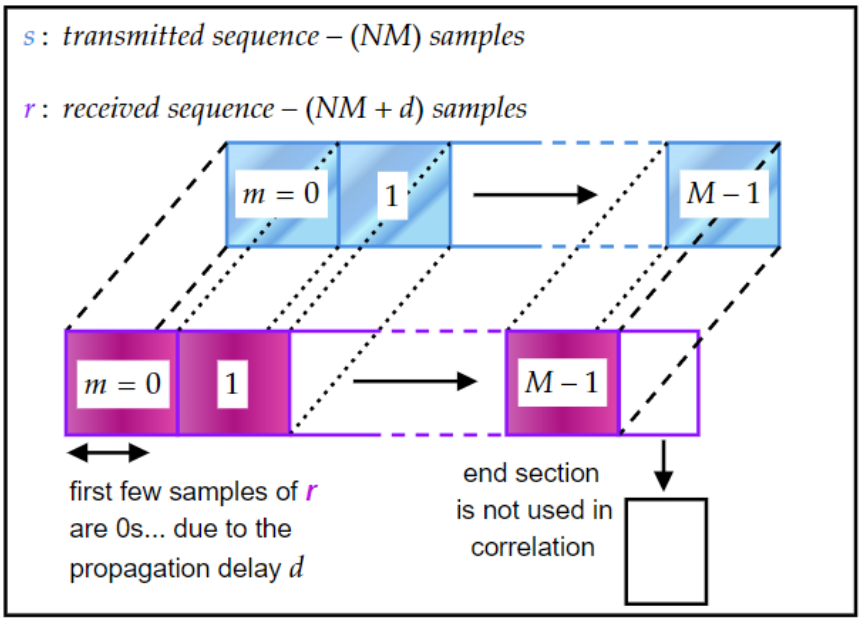

Fig. 4.4. Segmentation of the transmit and receive sequences to more easily allow for block-by-block processing.

The sequence s_m is equivalent to the m-th column of $\mathbf{F_{Tx}}$, and r_m equals the m-th column of $\mathbf{F_{Rx}}$. The two-dimensional cross-correlation between the two sequences can be expressed as

$$\chi_m(d, f) = \sum_{n=0}^{N-1} r_m[n] s_m^*[n-d] e^{-j2\pi f \frac{n}{P}}, \tag{4.13}$$

where n is the discrete-time index variable, and P is the extended OFDM symbol length, and equal to $N + GN$. When (4.13) is computed for each of the M symbols, a new intermediate matrix is obtained with (M) rows, and $(2N-1)$ columns - where

$(2N-1)$ is the length of the result of cross-correlating s_m and r_m.

$$\chi^{'}(d,f) = \begin{pmatrix} e_{0,0} & e_{0,1} & \cdots & e_{0,2N-1} \\ e_{1,0} & e_{1,1} & \cdots & e_{1,2N-1} \\ \vdots & \vdots & \ddots & \vdots \\ e_{M-1,0} & e_{M-1,1} & \cdots & e_{M-1,2N-1} \end{pmatrix} \tag{4.14}$$

The rows of this matrix can then be used to obtain the overall two-dimensional cross-correlation of the sequences s and r, as indicated in (4.15).

$$\chi_{r,s}(d,f) = \sum_{l=0}^{M-1} \chi_m^{'}(d,f) e^{-j2\pi fl} \tag{4.15}$$

To obtain the expression for the reciprocal filter from (4.15) only a small change in (4.13) is needed: instead of directly using the symbols of the transmit sequence (s), the reciprocal of each symbol or block (s_m) is first taken. Let the new sequence be denoted by $s_m^{'}$, where

$$s_m^{'} = 1/s_m^{*}. \tag{4.16}$$

This new sequence, $s_m^{'}$, then replaces s_m in (4.13).

Chapter 5

DFT-Spread OFDM Radar

As discussed in section 3.1, one of the main drawbacks of the orthogonal frequency-division multiplexing (OFDM) scheme is its high peak-to-average power ratio (PAPR). The high PAPR, which is induced by the Inverse Discrete Fourier Transform (IDFT) stage in the transmitter, can lead to undesirable distortions of the waveform during transmission [23]. Distortion of the waveform during transmission can lead to an increase in the communication system's bit error rate [24]. One method of mitigating this problem is that of Discrete Fourier Transform Spread (DFT-S) [29, 36, 37], also sometimes termed as DFT pre-coding. Before reviewing DFT-S, it is worth noting *why* it might be desirable to reduce the high PAPR of the OFDM waveform:

- Reducing the PAPR might facilitate the use of more inexpensive high-power amplifiers (HPAs) in the transmitter chain. This is because the demand for the HPA to have a highly linear characteristic would be lessened. This would be especially useful if there were multiple transmit antennas in use, like with

a MIMO-based radar system, as it would reduce hardware costs.

- The power consumption during transmission would be reduced. For small and mobile devices, this would aid in prolonging battery life.

The DFT-S technique involves first passing the set of transmit symbols - generated from a modulation alphabet such as QPSK, 16-QAM, 64-QAM etc. - through a Discrete Fourier Transform (DFT) block, *before* they are mapped to the inputs of an Inverse Discrete Fourier Transform (IDFT) block. The DFT stage is implemented efficiently using the FFT algorithm. Fig. 5.1 shows a simplified block diagram for a DFT-S OFDM system.

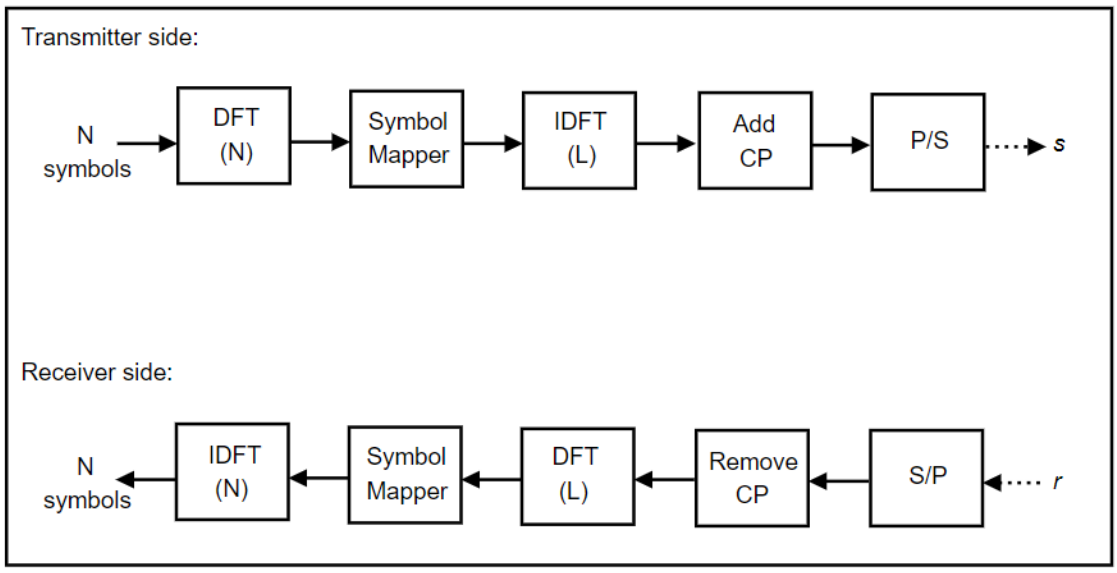

Fig. 5.1. Basic block diagram of a DFT-S OFDM System.

The DFT-S technique works on the basis that the size of the DFT and IDFT blocks are different - if they were the same then the IDFT operation would cancel

or negate the DFT's effect. The DFT block helps to mitigate the effect of the IDFT block (OFDM modulator) which is responsible for the high PAPR. The size of the IDFT block (L) is chosen to be an integer (K) multiple of the size of the DFT block - i.e., $L = KN$. This means one has some choice when mapping the N DFT outputs to the L IDFT inputs. Two mapping rules often used are *interleaving* and *localised* [37], [38]. Fig. 5.2-5.3 shows the basic characteristics of the methods of interleaving and localised mapping. When interleaving mapping is used, the N

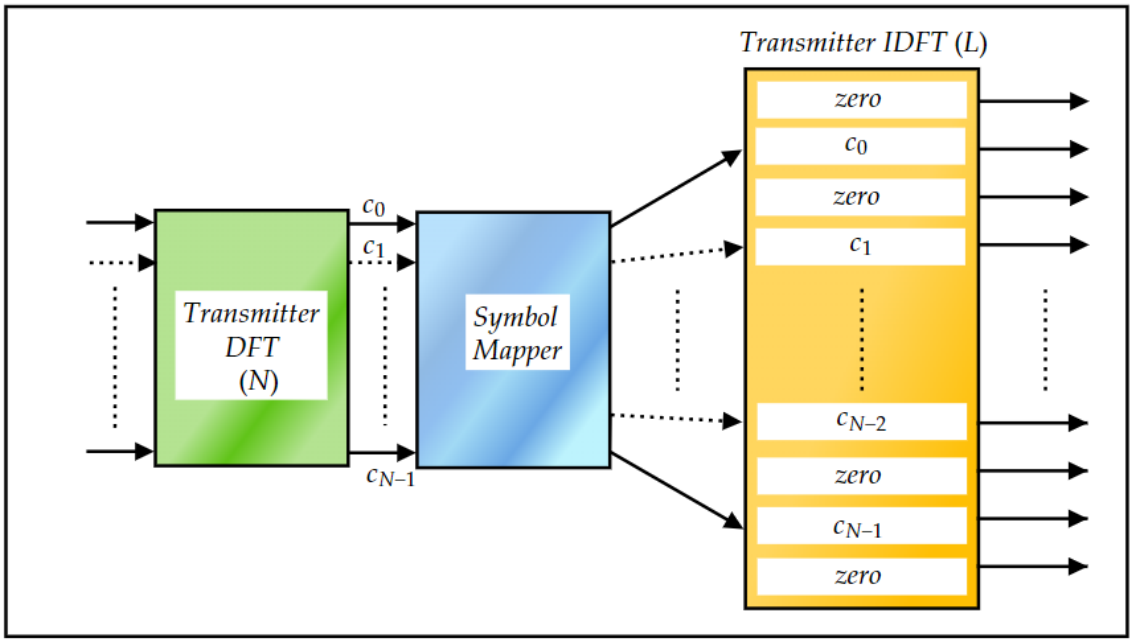

Fig. 5.2. Illustration of the idea of Interleaving Mapping.

output symbols from the DFT block are mapped over the whole set of L IDFT inputs, and the data symbols $[c_0, c_1, c_2, ..., c_{N-1}]$ are equally spaced out, with an appropriate number of zeros in between - for example, a single zero is inserted between each of the symbols in Fig. 5.2.

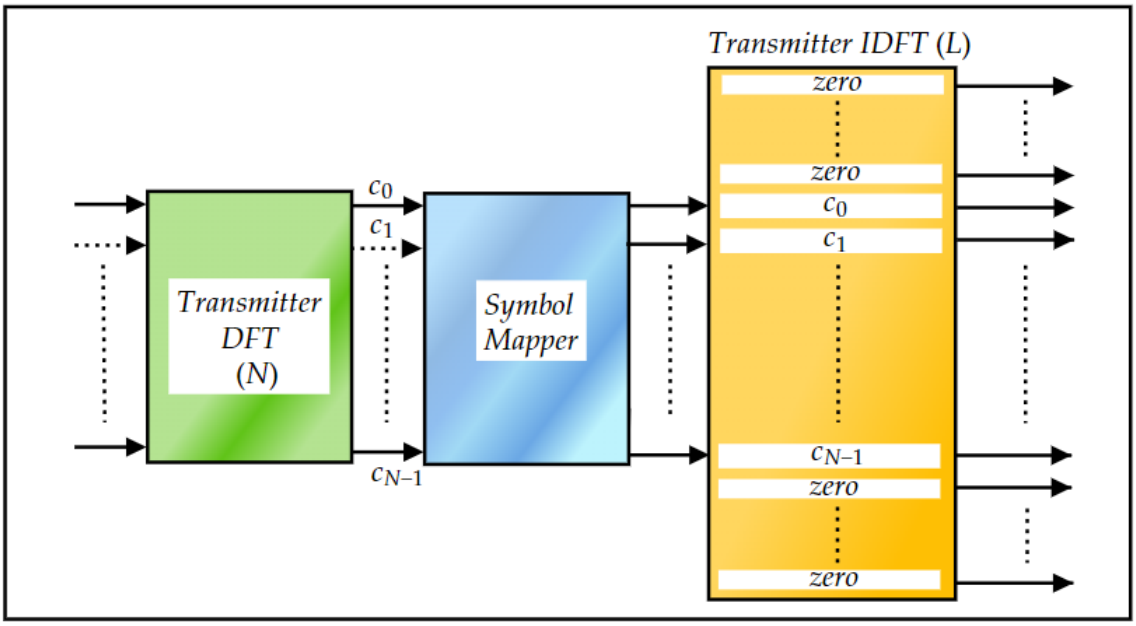

Fig. 5.3. Illustration of the idea of Localised Mapping.

Another benefit of the interleaving method of mapping is that if the channel gain is considerably low for a particular subcarrier, then there will likely be some number of null or idle subcarriers until the next active or occupied one. In this way, the overall throughput can be kept relatively high, even if one or two of the subcarriers have very low channel gains. With the localised method of mapping, if a given data subcarrier has a low channel gain, then its nearest neighbouring subcarriers are more likely to have low channel gains too. This can result in a continuous range of data subcarriers having a high bit error rate (BER).

Chapter 6

Simulation Results

6.1 DFT-Spread OFDM Radar

In this section, the effect of using the DFT-Spread (DFT-S) technique with the reciprocal-filter and periodogram-based algorithms will be investigated. The number of subcarriers (N) and OFDM symbols (M) will be varied, as well as the noise power. The effect of using the interleaving and localised mapping schemes is also investigated.

IEEE 802.11a and 802.11p Standards

The IEEE 802.11p standard is very widely used for ad hoc, inter-vehicular communications [39]. Considering that one of the potential applications of a joint OFDM-based communication and radar system is vehicles, the performance of the radar algorithms when this standard is used will be investigated in the simulations. The

performance obtained when the 802.11a standard is employed will also be considered, as it is widely used in communications. As a result, it will help to assess the compatibility of the OFDM waveform for both communications and radar purposes.

6.1.1 Reciprocal-filter Receiver

The first OFDM-based radar algorithm considered is that based on reciprocal filtering, as discussed at the end of section 4.3.

Interleaving Mapping

First, the interleaving method of mapping will be considered. The simulations were performed through MATLAB, and the parameters that were used are shown in Table 6.1. Fig. 6.1 shows the heat map generated by the reciprocal-filter (RF) receiver.

Number of subcarriers (N)	32, 52, 64
Number of OFDM symbols (M)	7, 10, 14
Modulation alphabet	16-QAM
Fraction of symbol used as CP (G)	0, 1/8
Noise power (dBW)	-25, -30, -40
IDFT size (L)	$2N$, $4N$
Signal attenuation (α)	$2 \times 10^{-3}, 6 \times 10^{-3}$

Table. 6.1. Simulation Parameters used in MATLAB Simulations.

The number of subcarriers (N) used was 64, and a total of 7 OFDM symbols were in the transmit sequence. The modulation scheme used was 16-QAM, and G was chosen to be 1/8. As can be seen in Fig. 6.1, it is not easy to discern the peak in the heat map located at the simulated delay (d_0) of 10 samples and Doppler shift

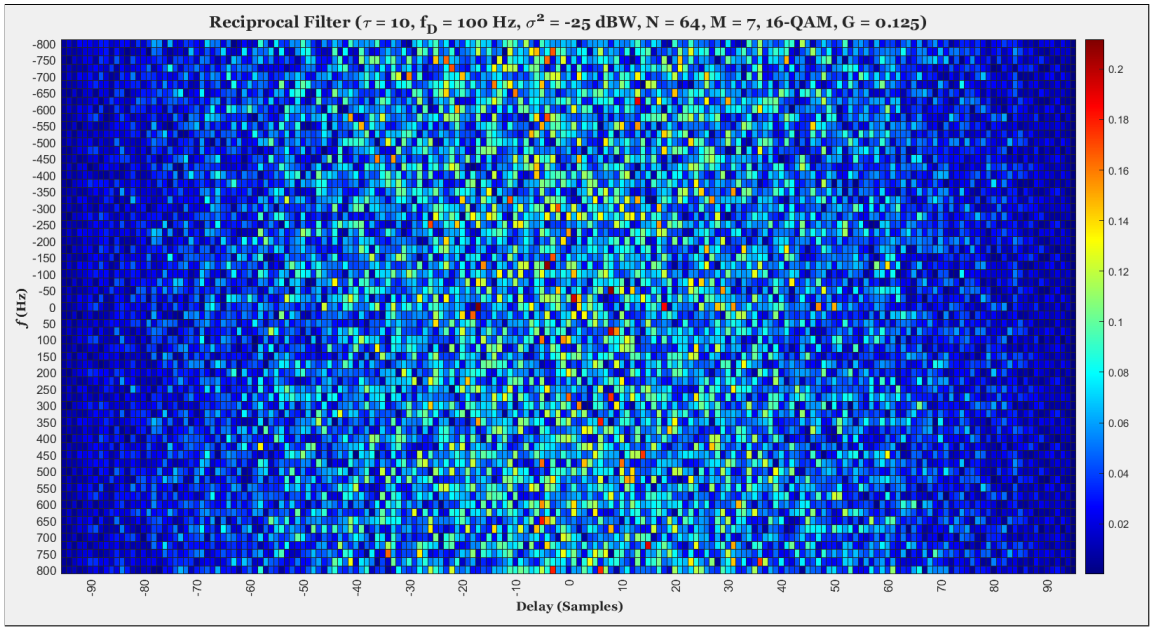

Fig. 6.1. Reciprocal-filter radar receiver, with no DFT-S on the transmit side.

(f_D) of 100 Hz. Considering Fig. 6.2, the red-coloured peak in the heat map is more easily picked out when the DFT-S technique is used. One promising advantage of the DFT-S technique on the transmitter side is the possibility of achieving an improved performance with a small number of data subcarrier channels (N) in use. Fig. 6.3 shows the heat map obtained when only 32 subcarriers are used ($N = 32$). It is seen that there is a strong correlation at a delay (d_0) of 10 samples, and a Doppler shift (f_D) of 100 Hz. However, there are some ambiguous peaks in the heat map, like in the previous case. This makes the decision-making process at the receiver difficult. Comparing this with Fig. 6.4, it is seen that when DFT-S is implemented the red-coloured peak is much easier to spot in the resulting heat map. The size of the IDFT block (L) was set to be four times that of the DFT block - i.e., $L = 4N$. The DFT-S

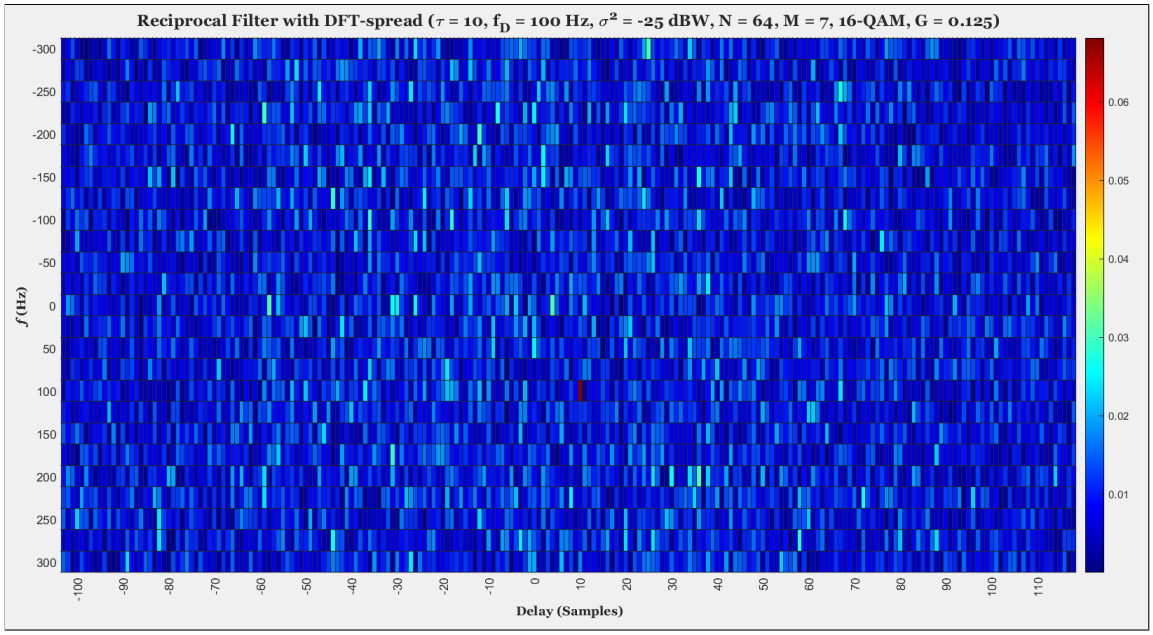

Fig. 6.2. Reciprocal-filter radar receiver **with** DFT-S on the transmit side. Zoomed in to improve visibility.

technique appears to have helped mitigate the effect of the additive White Gaussian noise. This would likely make the decision process for the radar receiver easier, and reduce the amount of post processing needed in order to identify the correct delay (d_0) and Doppler shift (f_D) values.

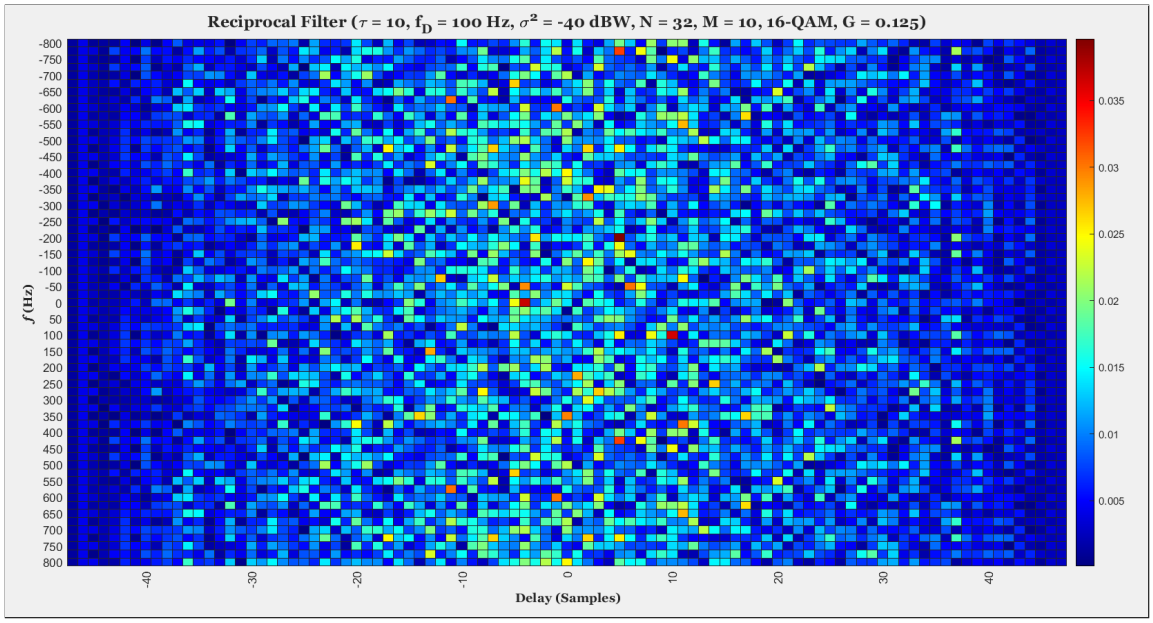

Fig. 6.3. Reciprocal-filter radar receiver with no DFT-S on the transmit side.

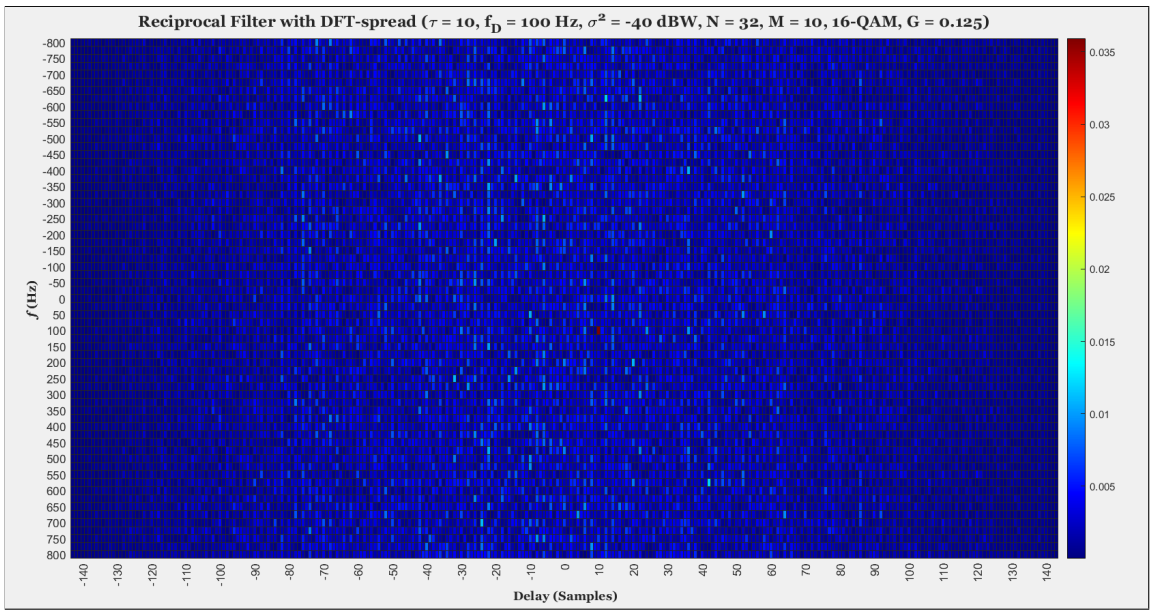

Fig. 6.4. Reciprocal-filter radar receiver **with** DFT-S on the transmit side.

Fig. 6.5 shows the heat map obtained when the 802.11a standard is used. The number of OFDM symbols (M) used was 14, and the fraction (G) of the OFDM symbol length taken as a cyclic prefix was 1/8. As is seen, the red-coloured peak is located at a delay (d_0) of 10 samples, and a Doppler shift (f_D) of 100 Hz. In Fig. 6.6,

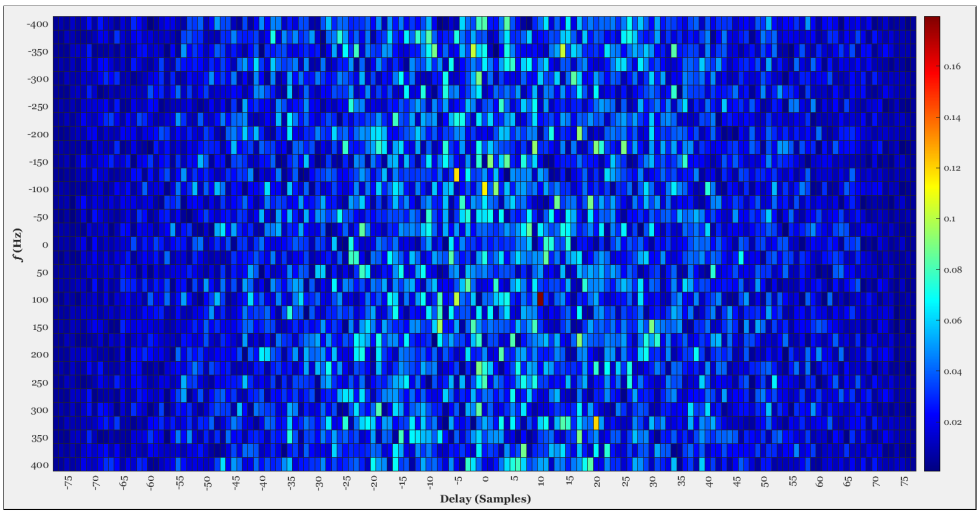

Fig. 6.5. 802.11a standard. No DFT-S is implemented. M = 14, G = 1/8.

where the DFT-S technique is employed, it is seen that the red-coloured peak is more easily discerned at the point (10, 100). Fig. 6.7 depicts the heat map obtained when the DFT-S technique is implemented and the 802.11p standard is used. Similar to Fig. 6.6, the red-coloured peak is more easily discerned.

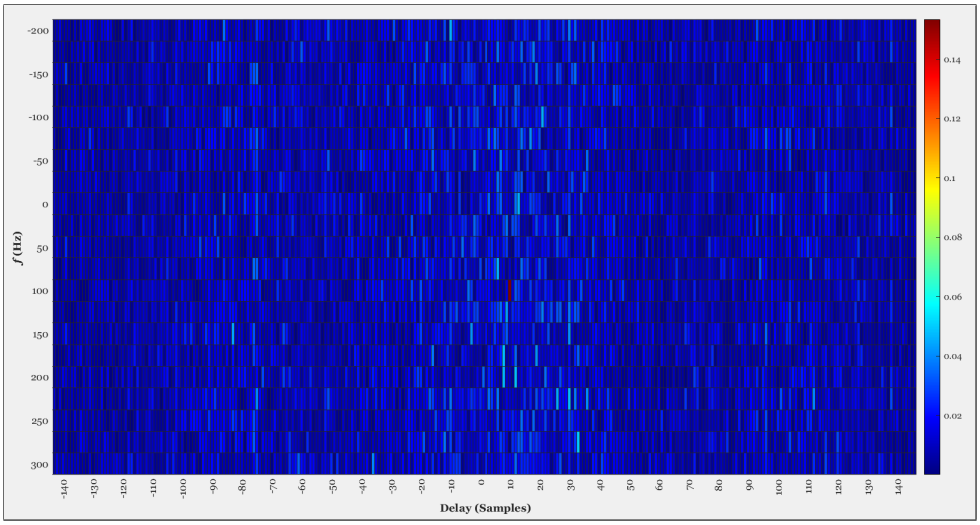

Fig. 6.6. 802.11a standard. DFT-S **is** implemented. Zoomed in to improve clarity. M = 14, G = 1/8.

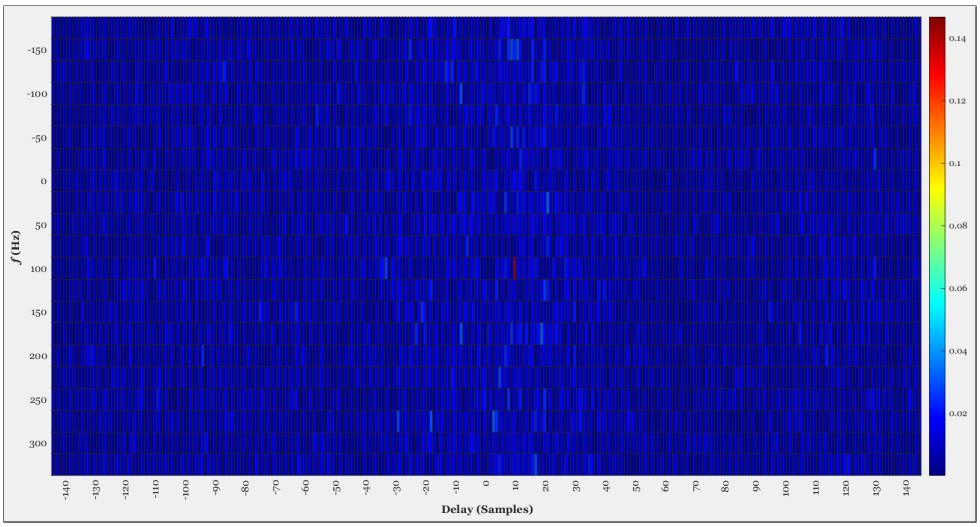

Fig. 6.7. 802.11p standard. DFT-S **is** implemented. Zoomed in to improve clarity. M = 14, G = 1/8.

Localised Mapping

Next, the effectiveness of localised mapping with the DFT-S technique will be investigated. In Fig. 6.8, the heat map obtained corresponds to when no DFT-S was employed at the transmitter. The number of subcarriers was set to 64 ($N = 64$), and 14 OFDM symbols were generated ($M = 14$). Like in the previous scenarios, 16-QAM was the modulation scheme used. The value of G was 1/8. In Fig. 6.8, it is

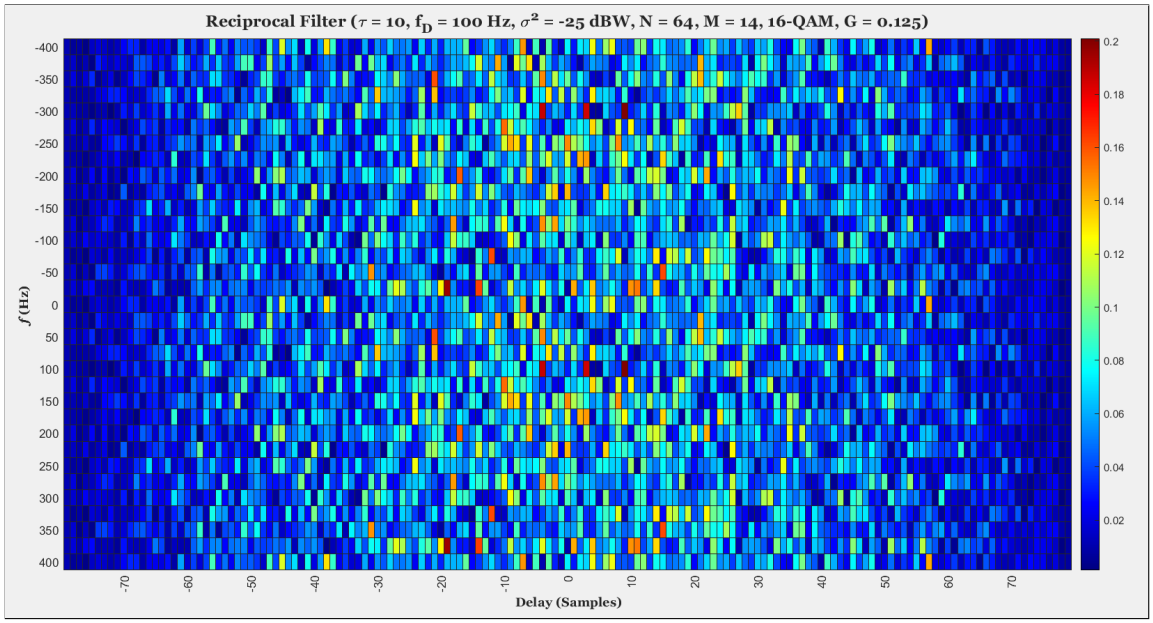

Fig. 6.8. Reciprocal filter with no DFT-S technique implemented on the transmitter side.

seen that there is a high correlation near the correct point (10,100) in the heat map. However, there are other points of high correlation, which makes the decision-making process for the radar receiver harder in this instance. This is in contrast to Fig. 6.9, where the heat map generated after employing DFT-S has a more discernible red

peak at the point (10,100). The IDFT size (L) was twice that of the DFT block (N). Lastly, it is worth illustrating that in some scenarios one might be able to use less

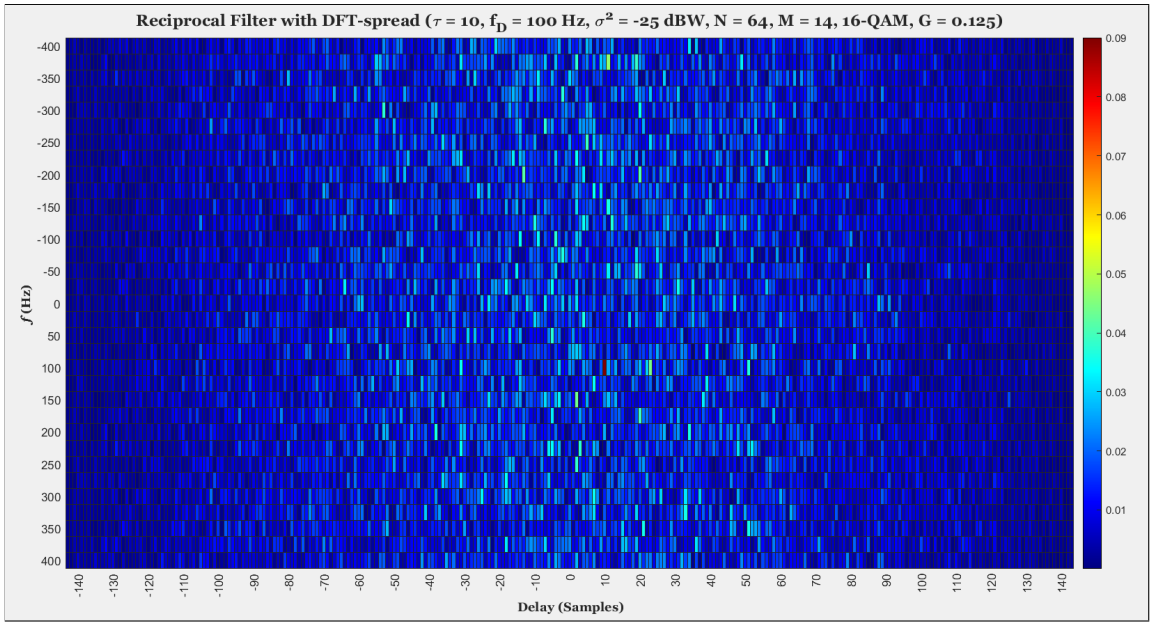

Fig. 6.9. Reciprocal filter **with** the DFT-S technique implemented on the transmitter side. $L = 2N = 128$.

active subcarriers (N) with the DFT-S technique *and* achieve an equal or improved performance. Fig. 6.10 shows the heat map for a reciprocal filter, without DFT-S used at the transmitter. The number of subcarriers (N) in use was 64. Comparing this with Fig. 6.11, which shows the heat map obtained when $N = 16$ and DFT-S is used, it is seen that the performance is no better in the first instance, when the number of subcarriers was 64 ($N = 64$). Fig. 6.12 shows the heat map generated by the RF receiver when the 802.11a standard is used, and DFT-S is implemented by the transmitter. The peak, corresponding to the simulated target parameters, is

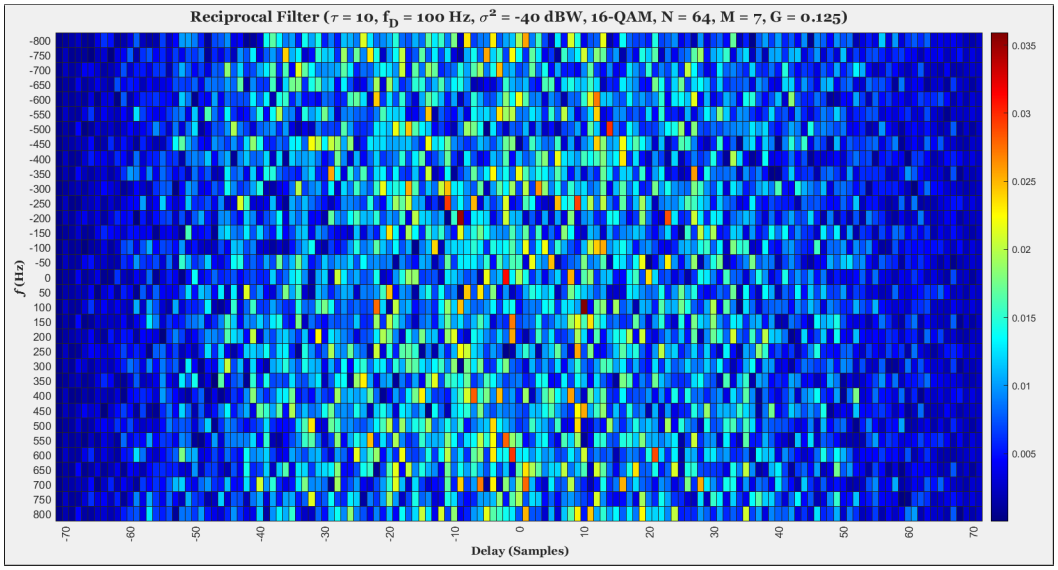

Fig. 6.10. Reciprocal filter with **no** DFT-S implemented, and **64** subcarriers in use.

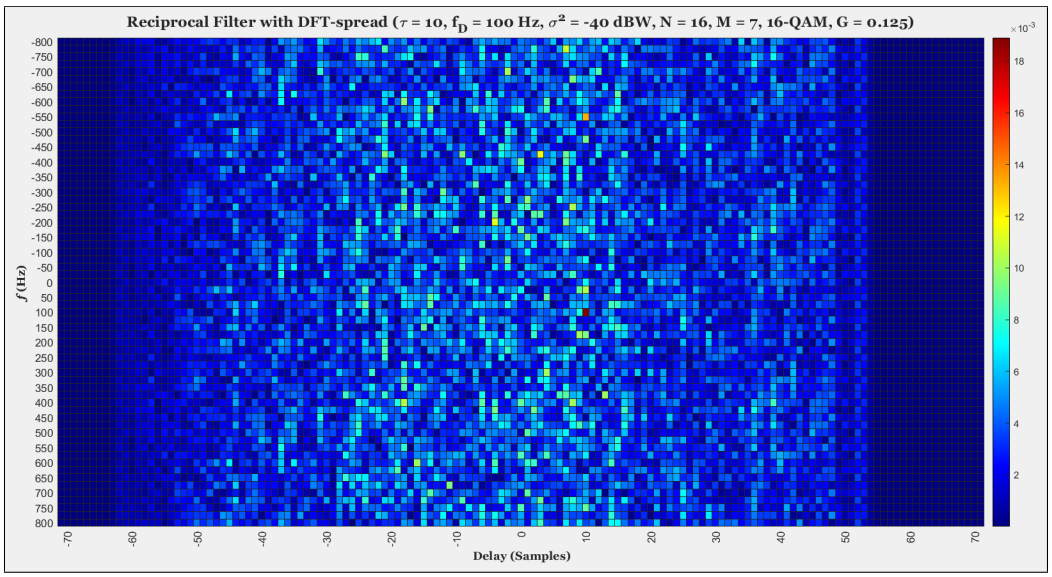

Fig. 6.11. Reciprocal filter **with** DFT-S implemented, and **16** active subcarriers in use.

more clearly defined when compared with Fig. 6.5, which corresponds to the case where the DFT-S technique is not used. Fig. 6.13 shows that, like before, the DFT-S technique also appears compatible in the case where the 802.11p standard is used.

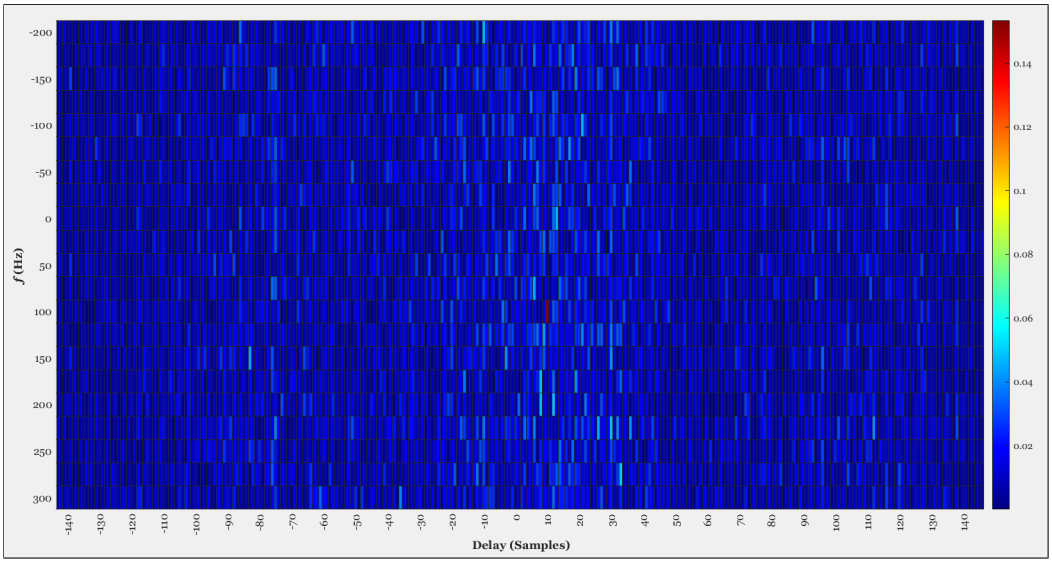

Fig. 6.12. 802.11a standard, **with** DFT-S implemented. Zoomed in to improve clarity. M = 14, G = 1/8.

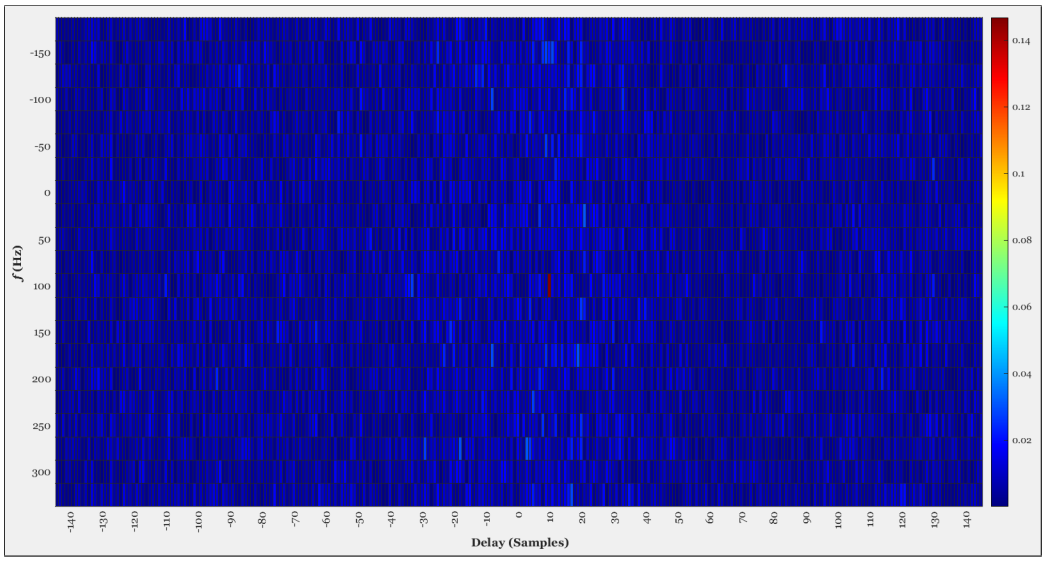

Fig. 6.13. 802.11p standard, **with** DFT-S implemented. Zoomed in to improve clarity. M = 14, G = 1/8.

6.1.2 Periodogram-based Receiver

The second OFDM-based radar algorithm considered is the periodogram-based one, also discussed in section 4.3. The simulation parameters that were used are shown in Table 6.2. The point-scatter model (6.1) was used to estimate the signal attenuation (α) associated with each target.

$$\alpha = \sqrt{\frac{c\sigma_{RCS}}{(4\pi)^3 d^4 f_C^2}}. \tag{6.1}$$

In (6.1), d denotes the distance to the target, f_C is the central frequency of the transmitted wave, σ_{RCS} represents the target's radar cross section (RCS), and c denotes the speed of light.

Number of subcarriers (N)	52
Number of OFDM symbols (M)	256
Modulation alphabet	16-QAM
Fraction of symbol used as CP (G)	1/8
Number of targets	2
Target distances (m)	30, 34
Target velocities (m/s)	60, 50
Target Radar Cross Sections (m^2)	10, 15
IDFT size (L)	$4N$
Signal attenuation (α)	$2.4 \times 10^{-10}, 2.3 \times 10^{-10}$

Table. 6.2. Simulation Parameters used in MATLAB Simulations of Periodogram-based Algorithm with DFT-S employed.

Fig. 6.14 depicts the range-Doppler map obtained when the periodogram-based algorithm is used with the 802.11a standard. The DFT-S technique is not used by the transmitter. As is seen, the two targets can be discerned. Comparing this to Fig. 6.15, it can be seen that the resolution is improved by the use of DFT-S, and the two targets can be more easily distinguished. This would likely result in an easier decision for the receiver, and produce more accurate estimates of each target's distance and velocity, as a result of the improved resolution. Fig. 6.16 shows the range-Doppler map generated when the 802.11p standard is used, and when no DFT-S is implemented by the transmitter. As is seen, with this standard, and the given target parameters, it is not possible to distinguish the two targets. This is in contrast to Fig. 6.17, where DFT-S is implemented, and the resolution is still sufficient to clearly discern each target in the range-Doppler map.

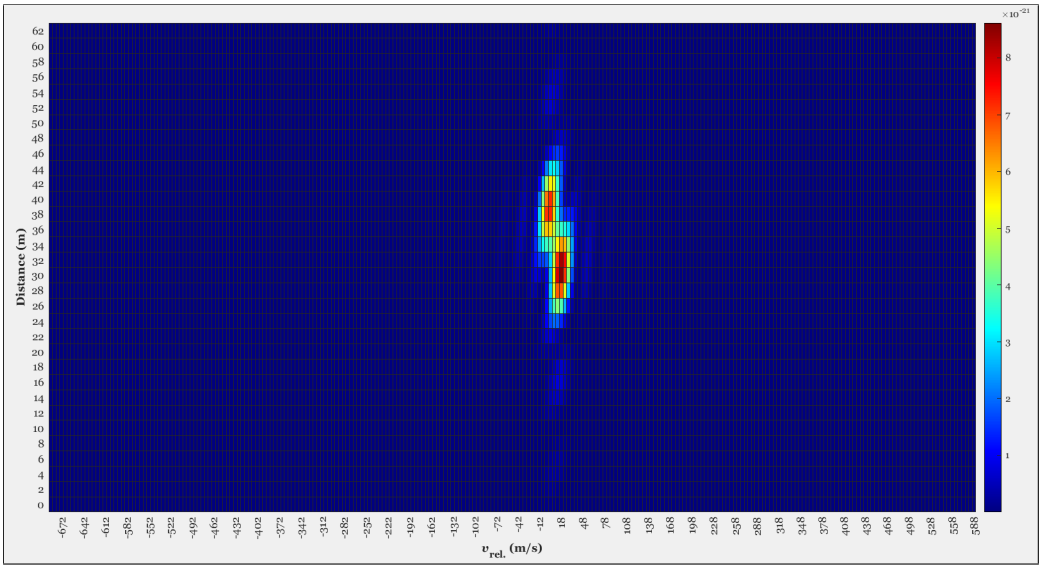

Fig. 6.14. Periodogram-based algorithm. The 802.11a standard was used.

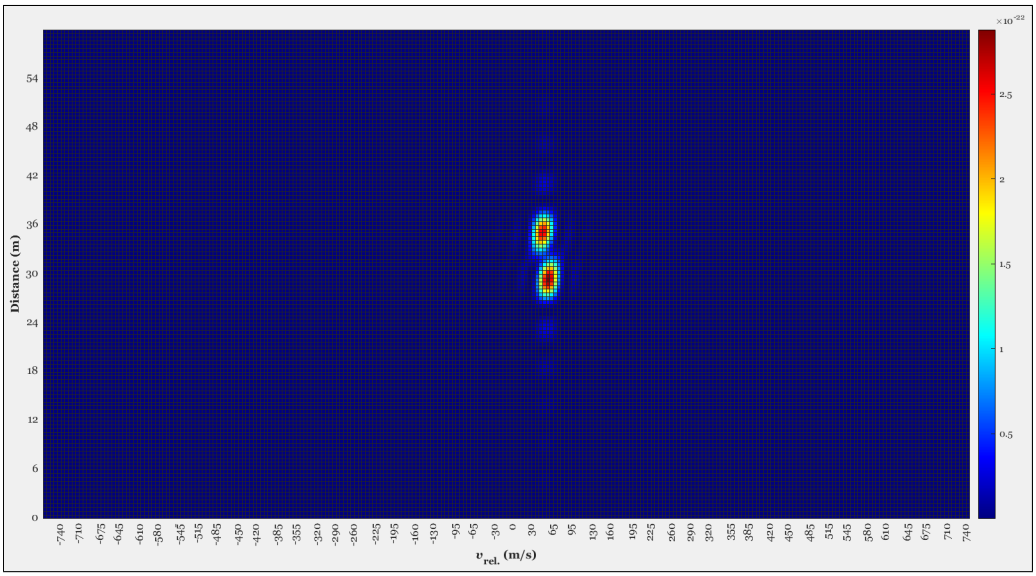

Fig. 6.15. Periodogram-based algorithm with DFT-S employed by the transmitter. The 802.11a standard was used.

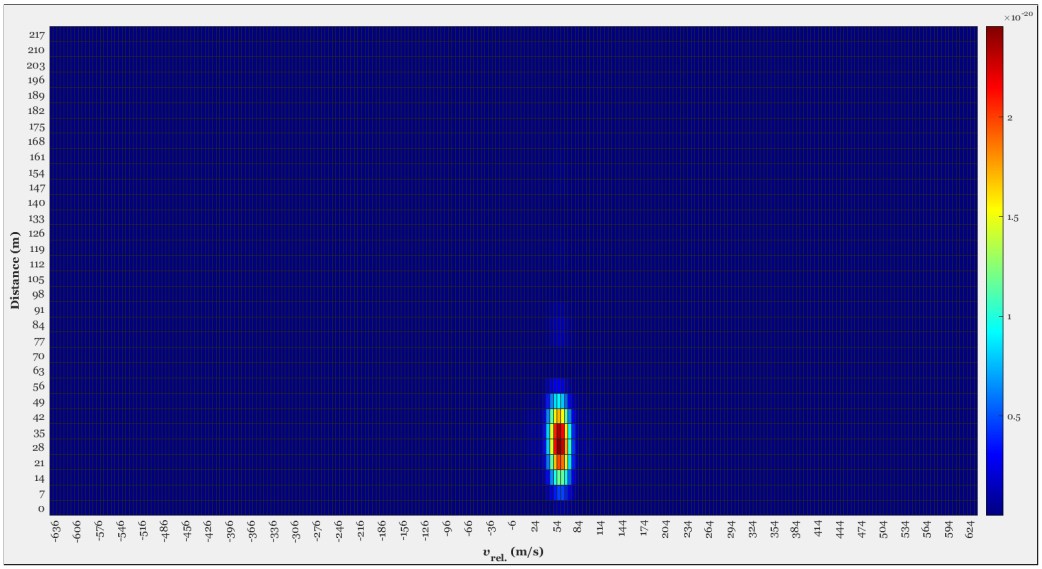

Fig. 6.16. Periodogram-based algorithm. The 802.11p standard was used.

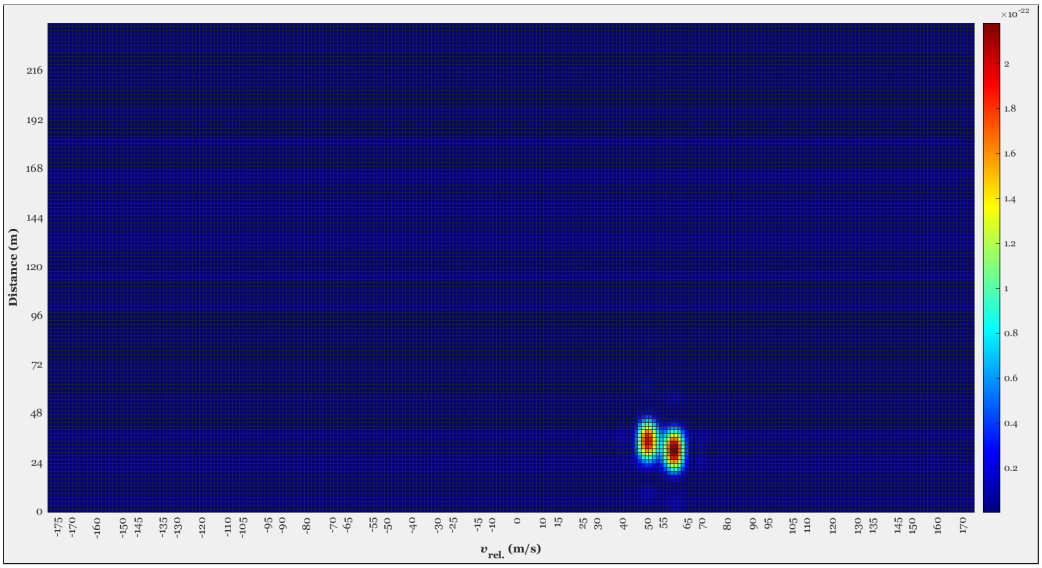

Fig. 6.17. Periodogram-based algorithm with DFT-S employed by the transmitter. The 802.11p standard used.

6.1.3 OFDM-based MIMO Radar

In this section, the effectiveness of using multiple transmit antennas is partly demonstrated. The simulations were performed through MATLAB, and the parameters used are shown in Table 6.3. Fig. 6.18 shows the heat map generated when the

Number of subcarriers (N)	52
Number of OFDM symbols (M)	14
Modulation alphabet	16-QAM
Fraction of symbol used as CP (G)	1/8
Noise power (dBW)	-30
IDFT size (L)	$4N$
Signal attenuation (α)	6×10^{-3}
Number of transmit antennas	4, 6
Delays of received signals	6, 6, 7, 7, 7, 7
Propagation delay (samples)	7
Doppler shift (f_D) (Hz)	250

Table. 6.3. Simulation Parameters used in MATLAB Simulations.

reciprocal-filter (RF) receiver is used. The red-coloured peak is identifiable at simulated delay and Doppler shift of 10 samples and 250 Hz. However, as can be seen, there are other points in the map which have similar intensity. Fig. 6.19 depicts the heat map obtained when the RF receiver is used with four transmit antennas. The DFT-S technique is also employed during transmission. As is seen, the red-coloured peak in the map is more distinguishable. Moreover, the ratio of the peak to the average intensity level is increased in this case. Fig. 6.20 shows the resulting heat map when six transmit antennas are employed. Similar to Fig. 6.19, the peak corresponding to the target parameters appears more discernible when compared to the case of a single transmit antenna.

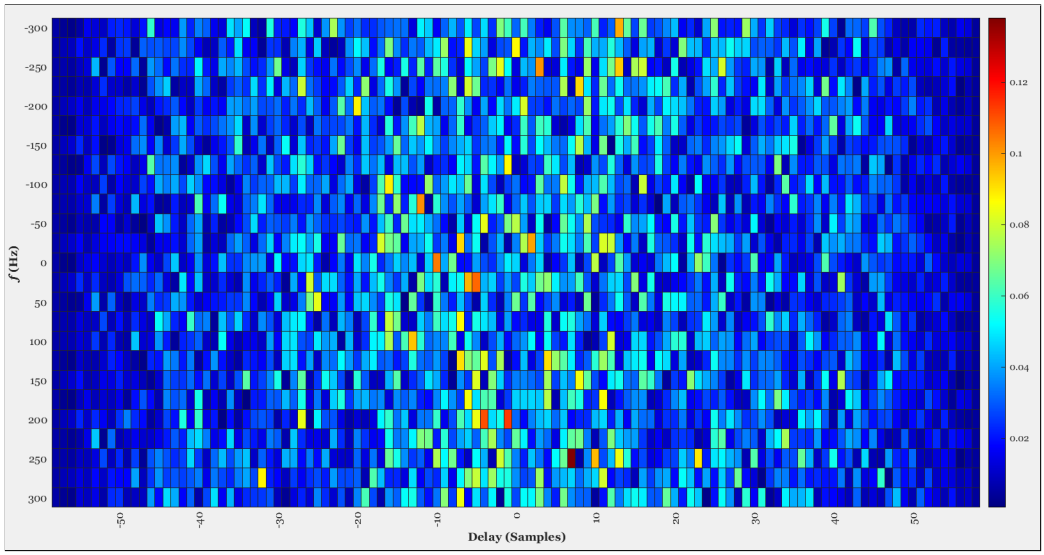

Fig. 6.18. The heat map generated for the reciprocal-filter receiver. One transmit antenna present.

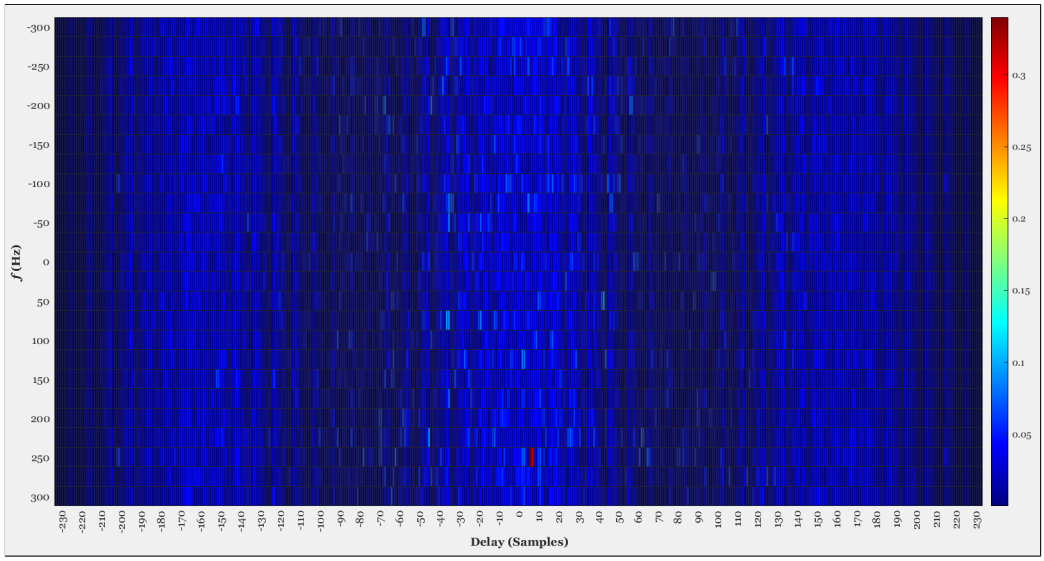

Fig. 6.19. The heat map generated for the reciprocal-filter receiver with DFT-S. **Four** transmit antennas used.

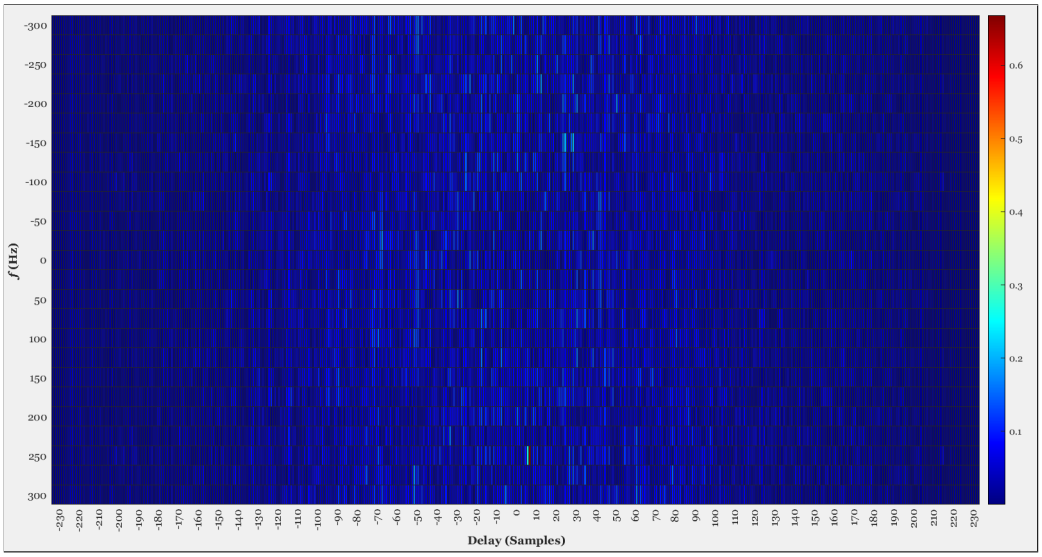

Fig. 6.20. The heat map generated for the reciprocal-filter receiver with DFT-S. **Six** transmit antennas used.

Inspecting the intensity values in the map, it seems that the use of multiple transmit antennas can help to increase the peak-to-sidelobes ratio.

Chapter 7

Conclusions

In this project it was shown that the method of Discrete Fourier Transform Spread (DFT-S) is compatible with correlation- and periodogram-based radar algorithms. This is promising for various reasons:

- In the case of correlation- and periodogram-based algorithms, the peak-to-average power ratio (PAPR) of the OFDM-based radar signal can be reduced without compromising the radar's performance.

- The DFT-Spread stage helps to put less demand on the high-power amplifier (HPA) used in the transmitter. This reduces the hardware costs, as the resulting amplifiers are less expensive to build.

- The DFT-Spread technique is already used in wireless communications, and so it is promising to see that the radar's performance is not hindered by its inclusion in the transmitter chain. It also gives promise to the idea of combining

both communications and radar functionality into a single system, which would bring many advantages, as discussed in the introduction.

- The scenarios simulated in this paper suggest that one might be able to use a lower number of active subcarriers (N) and achieve a better performance when the DFT-Spread technique is used (cf. Fig. 6.10 and 6.11).

- With localised mapping, the edge subcarriers are left idle. This can help protect against interference from other systems that use a similar section of the frequency spectrum.

A basic MIMO-based OFDM radar system using the DFT-Spread technique was simulated in MATLAB. The radar receiver used was based on reciprocal filtering, and the results indicate that a higher peak-to-sidelobe ratio can be achieved when multiple transmit antennas are used. Moreover, since each transmitter in a MIMO-based radar will likely have its own receiver, it is promising to see that the DFT-Spread is compatible, as it might help to allow more inexpensive high-power amplifiers to be used. This would likely lead to a considerable costs savings in a mass-production scenario.

7.1 Ethics and Sustainability

Since one of the potential applications of OFDM-based radar is in vehicles, health and safety would be of utmost importance. Testing of any future OFDM-radar technology would need to be broad and thorough, so as to avoid accidents or disasters in real-world settings. Testing constitutes a significant cost in both time and money throughout the development of a product or technology. An ethical concern might be that the testing phase is neglected or insufficiently done by commercial companies, which might lead to bugs or errors in real-world settings such as roads - this is especially important as investment in the autonomous vehicle sector continues to increase. The hardware and software associated with a potential OFDM communication-and-radar system would need to be maintained in order to keep pace with newer and newer autonomous vehicles.

7.2 Future Work

Some areas to explore in future work might be:

- Investigate the effectiveness of the DFT-Spread technique with other radar algorithms. This could also be undertaken with more realistic channel models.
- Investigate other mapping techniques. For example, the distributed method of mapping the outputs from the DFT block to the inputs of the IDFT block.
- In this project, due to time constraints, a very basic model for the MIMO-based radar was considered. In the future, other algorithms like MUSIC or ESPRIT

could be investigated. Estimation of a target's azimuth angle could also be undertaken.

- An analysis of a MIMO-based radar system where each transmit antenna is processing the received signals using different algorithms, before a final processing of the outputs.

Bibliography

[1] "Digital Video Broadcasting (DVB); Framing Structure, Channel Coding and Modulation for Digital Terrestrial Television (DVB-T)," European Telecommunications Standards Institute (ETSI), Standard, Mar. 2008-09.

[2] B. Ouarzazi, M. Berbineau, I. Dayoub, and A. Menhaj-Rivenq, "Channel estimation of ofdm system for high data rate communications on mobile environments," in *2009 9th International Conference on Intelligent Transport Systems Telecommunications, (ITST)*, 2009, pp. 425–429.

[3] "Ieee standard for information technology—telecommunications and information exchange between systems local and metropolitan area networks—specific requirements," *IEEE Std 802.11-2016 (Revision of IEEE Std 802.11-2012)*, 2016.

[4] "Timeline from 1g to 5g: A brief history on cell phones," https://www.cengn.ca/information-centre/innovation/timeline-from-1g-to-5g-a-brief-history-on-cell-phones/.

[5] W. Ejaz, A. Anpalagan, M. A. Imran, M. Jo, M. Naeem, S. B. Qaisar, and W. Wang, "Internet of things (iot) in 5g wireless communications," *IEEE Access*, vol. 4, pp. 10 310–10 314, 2016.

[6] F. Liu, C. Masouros, A. P. Petropulu, H. Griffiths, and L. Hanzo, "Joint radar and communication design: Applications, state-of-the-art, and the road ahead," *IEEE Transactions on Communications*, vol. 68, no. 6, pp. 3834–3862, 2020.

[7] N. Levanon, "Multifrequency complementary phase-coded radar signal," *Radar, Sonar and Navigation, IEE Proceedings* -, vol. 147, pp. 276 – 284, 01 2001.

[8] G. Lellouch and H. Nikookar, "On the capability of a radar network to support communications," in *2007 14th IEEE Symposium on Communications and Vehicular Technology in the Benelux*, 2007, pp. 1–5.

[9] G. Franken, H. Nikookar, and P. V. Genderen, "Doppler tolerance of ofdm-coded radar signals," in *2006 European Radar Conference*, 2006, pp. 108–111.

[10] M. Ruggiano and P. van Genderen, "Wideband ambiguity function and optimized coded radar signals," in *2007 European Radar Conference*, 2007, pp. 142–145.

[11] C. Sturm, T. Zwick, and W. Wiesbeck, "An ofdm system concept for joint radar and communications operations," in *VTC Spring 2009 - IEEE 69th Vehicular Technology Conference*, 2009, pp. 1–5.

[12] C. Sturm and W. Wiesbeck, "Waveform design and signal processing aspects for fusion of wireless communications and radar sensing," *Proceedings of the IEEE*, vol. 99, no. 7, pp. 1236–1259, 2011.

[13] C. Sturm, T. Zwick, W. Wiesbeck, and M. Braun, "Performance verification of symbol-based ofdm radar processing," in *2010 IEEE Radar Conference*, 2010, pp. 60–63.

[14] K. M. Braun, "Ofdm radar algorithms in mobile communication networks," Ph.D. dissertation, Karlsruhe, Karlsruher Institut für Technologie (KIT), Diss., 2014, 2014.

[15] S. Mercier, S. Bidon, D. Roque, and C. Enderli, "Comparison of correlation-based ofdm radar receivers," *IEEE Transactions on Aerospace and Electronic Systems*, vol. 56, no. 6, pp. 4796–4813, 2020.

[16] H. F. Arrano and C. A. Azurdia-Meza, "Ofdm: today and in the future of next generation wireless communications," in *2016 IEEE Central America and Panama Student Conference (CONESCAPAN)*, 2016, pp. 1–6.

[17] P. Malathi and P. Vanathi, "Orthogonal frequency division multiplexing (ofdm) for wireless local area network (wlan)," *International Journal of Advancement of Modeling & Simulation techniques in Enterprises (AMSE)*, vol. 51, pp. 1–16, 01 2008.

[18] B. Li, Q. Qu, Z. Yan, and M. Yang, "Survey on ofdma based mac protocols for the next generation wlan," in *2015 IEEE Wireless Communications and Networking Conference Workshops (WCNCW)*, 2015, pp. 131–135.

[19] A. Agarwal and S. K. Patra, "Performance prediction of ofdm based digital audio broadcasting system using channel protection mechanisms," in *2011 3rd International Conference on Electronics Computer Technology*, vol. 2, 2011, pp. 57–61.

[20] Z. Wang, T. Mao, and Q. Wang, "Optical ofdm for visible light communications," in *2017 13th International Wireless Communications and Mobile Computing Conference (IWCMC)*, 2017, pp. 1190–1194.

[21] M. Afgani, H. Haas, H. Elgala, and D. Knipp, "Visible light communication using ofdm," in *2nd International Conference on Testbeds and Research Infrastructures for the Development of Networks and Communities, 2006. TRIDENTCOM 2006.*, 2006, pp. 6 pp.–134.

[22] Y. S. Cho, J. Kim, W. Y. Yang, and C.-G. Kang, *MIMO-OFDM Wireless Communications with MATLAB*. Wiley, 2010.

[23] A. Bo, Y. Zhi-xing, P. Chang-yong, Z. Tao-tao, and G. Jian-hua, "Effects of papr reduction on hpa predistortion," *IEEE Transactions on Consumer Electronics*, vol. 51, no. 4, pp. 1143–1147, 2005.

[24] Y. Rahmatallah and S. Mohan, "Peak-to-average power ratio reduction in ofdm systems: A survey and taxonomy," *IEEE Communications Surveys Tutorials*, vol. 15, no. 4, pp. 1567–1592, 2013.

[25] K. Tani, Y. Medjahdi, H. Shaiek, R. Zayani, and D. Roviras, "Papr reduction of post-ofdm waveforms contenders for 5g amp; beyond using slm and tr algorithms," in *2018 25th International Conference on Telecommunications (ICT)*, 2018, pp. 104–109.

[26] N. Ohkubo and T. Ohtsuki, "Design criteria for phase sequences in selected mapping," in *The 57th IEEE Semiannual Vehicular Technology Conference, 2003. VTC 2003-Spring.*, vol. 1, 2003, pp. 373–377 vol.1.

[27] F. Tosato, M. Sandell, and M. Tanahashi, "Tone reservation for papr reduction: An optimal approach through sphere encoding," in *2016 IEEE International Conference on Communications (ICC)*, 2016, pp. 1–6.

[28] M. F. Pervej, M. Z. I. Sarkar, T. K. Roy, M. M. Hasan, M. M. Rahman, and S. K. Bain, "Analysis of papr reduction of dft-scfdma system using different subcarrier mapping schemes," in *2014 17th International Conference on Computer and Information Technology (ICCIT)*, 2014, pp. 435–439.

[29] R. Ahmad and A. Srivastava, "Papr reduction of ofdm signal through dft precoding and gmsk pulse shaping in indoor vlc," *IEEE Access*, vol. 8, pp. 122 092–122 103, 2020.

[30] M. A. E. Mofeed and H. A. Elsalam Mofeed, "Direction-of-arrival methods (doa) and time difference of arrival (tdoa) position location technique," in *Proceedings of the Twenty-Second National Radio Science Conference, 2005. NRSC 2005.*, 2005, pp. 173–182.

[31] E. Fishler, A. Haimovich, R. Blum, D. Chizhik, L. Cimini, and R. Valenzuela, "Mimo radar: an idea whose time has come," in *Proceedings of the 2004 IEEE Radar Conference (IEEE Cat. No.04CH37509)*, 2004, pp. 71–78.

[32] B. J. Donnet and I. D. Longstaff, "Combining mimo radar with ofdm communications," in *2006 European Radar Conference*, 2006, pp. 37–40.

[33] M. Braun, C. Sturm, and F. K. Jondral, "Maximum likelihood speed and distance estimation for ofdm radar," in *2010 IEEE Radar Conference*, 2010, pp. 256–261.

[34] ——, "On the single-target accuracy of ofdm radar algorithms," in *2011 IEEE 22nd International Symposium on Personal, Indoor and Mobile Radio Communications*, 2011, pp. 794–798.

[35] S. Searle, J. Palmer, L. Davis, D. W. O'Hagan, and M. Ummenhofer, "Evaluation of the ambiguity function for passive radar with ofdm transmissions," in *2014 IEEE Radar Conference*, 2014, pp. 1040–1045.

[36] S. Ahmadi, *5G NR: architecture, technology, implementation, and operation of 3GPP new radio standards.* Academic Press, 2019.

[37] K. Tahkoubit, A. Ali-Pacha, H. Shaiek, and D. Roviras, "Papr reduction of bf-ofdm waveform using dft-spread technique," in *2019 16th International Symposium on Wireless Communication Systems (ISWCS)*, 2019, pp. 406–410.

[38] Z.-Y. Wu, G. Yu-Liang, Z.-K. Wang, C. You, C. Yang, C. Luo, and J. Wang, "Optimized dft-spread ofdm based visible light communications with multiple lighting sources," *Optics Express*, vol. 25, p. 26468, 10 2017.

[39] P. Papadimitratos, A. D. La Fortelle, K. Evenssen, R. Brignolo, and S. Cosenza, "Vehicular communication systems: Enabling technologies, applications, and future outlook on intelligent transportation," *IEEE Communications Magazine*, vol. 47, no. 11, pp. 84–95, 2009.

Appendix D: Hazard Identification / Risk Analysis

SCHOOL OF ELECTRICAL & ELECTRONIC ENGINEERING

ME ELECTRICAL POWER ENGINEERING
or ME ELECTRONIC & COMPUTER ENGINEERING

Please submit this signed form through Brightspace within **2 weeks** of your project being assigned.

At the end of the project, you must include a copy of this form in your final report. Note that **you may need to update the form** if new circumstances arise relating to safety during the course of the project.

Scan and email the original form to yourself with the Subject line "Hazard identification Risk Analysis Stamped", for easy retrieval at the end of the Spring trimester when submitting your final report.

Student Name:	Dylan Boland	Signature DKB
Student Number:	17734349	
Supervisor:	Dr Nam Tran	Signature
Project Title:	OFDM-based Joint Radar and Communication	
Programme:	ME in Electronic and Computer Engineering	

Identify any potential safety hazards for your project, e.g. dangerous voltages, rotating machinery, radiation, soldering fumes, sitting in front of a computer for prolonged periods

As my project entails programming and simulating, there are no serious risks in my case.

Indicate how all identified safety hazards will be managed to provide a safe working environment

N/A